ULTRA – HIGH STRENGTH STEEL COLUMNS UNDER ELEVATED TEMPERATURES

LUCCA GIOVANE CONSTANTE

Dissertation Submitted to the Polytechnic Institute of Bragança (Portugal) with the Federal University of Technology - Paraná (Brazil) to the fulfilment of the Requirements for the Double Diploma program to obtain the degree of

Master degree in Construction Engineering

Supervised by:

Prof. Doctor Paulo Alexandre Gonçalves Piloto

Prof. Doctor Paola Regina Dalcanal

This dissertation does not include the comments and suggestions mentioned by the Jury.

BRAGANÇA 2023-2024

Declaro que o trabalho descrito neste relatório é da minha autoria e é da minha vontade que o mesmo seja submetido a avaliação.

Lucca Giovane Constante – a57035

CONTENTS

LIST OF FIGURES

LIST OF TABLES

DEDICATORY

For the relentless pursuit of knowledge and unwavering dedication of structural engineering, this work is dedicated to all those who tirelessly seek to ensure the safety and resilience of our built environment. In memory of those who have suffered the devastating consequences of structural failure in fire conditions, and with a deep commitment to preventing such tragedies in the future.

ACKNOWLEDGEMENT

First of all, I thank God, for the opportunities that gives to me, like that one specifically, witch study in another country and know about other cultures, make new friends and get experiences that will be so good for me for all my life. After that, I would like to express my deepest gratitude to the following people and institutions, whose support and contributions have made this incredible research possible:

I want to express my heartfelt gratitude to my family, Jilvani (in memorian), Geane, Vinicius, Maria Eduarda, Daryane and friends for patience, encouragement, and unwavering belief in my capacities. Your emotional support sustained me through the challenges of this academic journey.

Paulo Piloto, I need to thank your guidance, expertise, and unwavering support throughout this research journey have been instrumental in shaping this work. Your mentorship has been a source of inspiration, and I am grateful for the opportunities to learn from you. Paola, thank you for the necessary support the times I got in touch and for agreeing to be my co-supervisor, you were also important in this journey.

To Federal University of Paraná and Polytechnique Institute of Bragança, which has provided a conducive environment for research and learning. I appreciate the resources and opportunities provided by those institutions.

To my Revest Solutions and DST colleagues, for the support, patience and, above of all, the opportunity they gave me throughout this journey.

Last but not least, I acknowledge the countless individuals whose work and research in the field of structural engineering and fire safety have laid the foundation for this study. Your contributions have been indispensable.

Lucca Constante.

Thank you.

AGRADECIMENTOS

Em primeiro lugar, agradeço a Deus, pelas oportunidades que me dá, como esta especificamente, de estudar em outro país e conhecer diferentes culturas, fazer novos amigos e obter experiências que me serão tão boas para toda a vida. Depois disso, gostaria de expressar a minha mais profunda gratidão às seguintes pessoas e instituições, cujo apoio e contribuições tornaram possível esta incrível investigação:

Quero expressar a minha sincera gratidão à minha família, Jilvani (in memorian) Geane, Vinicius, Maria Eduarda, Daryane e amigos por toda paciência, encorajamento e crença inabalável nas minhas capacidades. O vosso apoio emocional sustentou-me durante os desafios deste percurso académico.

Paulo Piloto, tenho de agradecer a sua orientação, experiência e apoio inabalável ao longo deste percurso de investigação, que foram fundamentais para dar forma a este trabalho. A tua orientação tem sido uma fonte de inspiração e estou grato pelas oportunidades de aprender contigo. Paola, obrigado pelo suporte necessário nas vezes em que entrei em contato e por ter aceitado ser minha co-orientadora, você também teve importância nesta jornada.

À Universidade Federal do Paraná e ao Instituto Politécnico de Bragança, que proporcionaram um ambiente propício à pesquisa e ao aprendizado. Agradeço os recursos e as oportunidades oferecidas por essas instituições.

Aos colegas da Revest Solutions e DST, pelo apoio, paciência e, principalmente, pela oportunidade que me deram ao longo desta jornada.

Por último, mas não menos importante, agradeço às inúmeras pessoas cujo trabalho e investigação no domínio da engenharia estrutural e da segurança contra incêndios lançaram as bases para este estudo. Os vossos contributos foram indispensáveis.

Lucca Constante.

Obrigado.

RESUMO

A avaliação do comportamento estrutural de colunas de aço sob condições extremas, como incêndios, é crucial para garantir a segurança e a integridade das edificações. Este estudo investiga o desempenho de colunas circulares fabricadas com aço de ultra alta resistência (UHSS) quando submetidas a temperaturas elevadas provocadas por incêndios. Utilizando a ferramenta de análise de elementos finitos, ANSYS Mechanical APDL, foram conduzidas ao todo 15 simulações detalhadas para modelar e analisar a resposta térmica e estrutural de uma coluna CHS (Circular Hollow Section) de um aço com tensão de cedência de 1200 MPa, com diâmetro e espessura de 76.1 mm e 3.1 mm, respetivamente. Com dados extraídos de um teste experimental realizado por Farmani et al., a pesquisa foca em aspectos como a distribuição de temperatura, as tensões induzidas pelas temperaturas elevadas e a capacidade de carga da coluna para analisar seu tempo de resistência e temperatura de falha sob diferentes cenários de incêndio. Foram utilizadas, para além das curvas de temperaturas obtidas no ensaio experimental com taxas de aquecimento de 5 ºC/min e 20 ºC/min, as curvas de incêndio padrão ISO 834 e a curva de incêndios de hidrocarbonetos (combustíveis fósseis, por exemplo). Os resultados obtidos fornecem uma compreensão aprofundada do comportamento mecânico das colunas de UHSS em situações de incêndio, oferecendo dados valiosos para a engenharia de segurança contra incêndios e para o projeto de estruturas mais resilientes, onde fica evidente o feito da taxa de aquecimento no tempo de resistência ao fogo, considerando o nível de carga do elemento.

Palavras-chave: Aço de Ultra Alta Resistência; Colunas; Incêndio; Análise de elementos finitos.

ABSTRACT

The evaluation of the structural behaviour of steel columns under extreme conditions, such as fires, is crucial for ensuring the safety and integrity of buildings. This study investigates the performance of circular columns made of Ultra-High-Strength Steel (UHSS) when subjected to high temperatures caused by fires. Using the finite element analysis software ANSYS Mechanical APDL, a total of 15 detailed simulations were conducted to model and analyse the thermal and structural response of a CHS (Circular Hollow Section) column made of steel with a yield strength of 1200 MPa, with a diameter and thickness of 76.1 mm and 3.1 mm, respectively. Using data extracted from an experimental test conducted by Farmani et al., the research focuses on temperature distribution, heat-induced stresses, and the load-bearing capacity of the column to analyse its resistance time and failure temperature under different fire scenarios. In addition to the temperature curves obtained from the experimental test, using heating rates of 5 and 20 ºC/min, this study uses the standard fire ISO 834 and the hydrocarbon fire (e.g., fossil fuels). The results provide an in-depth understanding of the mechanical behaviour of UHSS columns in fire situations, offering valuable data for fire safety engineering and the design of more resilient structures, where the effect of the heating rate over time is evident on the fire resistance, considering the load level of the element.

Keywords: Ultra-Hight Strength Steel; Columns; Fire; FE analysis.

1- INTRODUCTION

1.1- Framework

Steel constructions are gaining notoriety among the different construction methods due to their highly beneficial properties, such as strength, workability, durability and elasticity. For this reason, it has been the subject of study for the last few years.

These properties above provide advantages in terms of reducing costs and execution time, as well as making it possible to construct long-span structures, high-rise buildings and structural elements (beams and columns) with higher slenderness indexes, when a reinforced concrete solution, for example, would be more expensive and time-consuming, presenting a lower cost-benefit ratio compared to steel.

In recent years, progress in the development of Ultra-High-Strength steels has become a crucial area of research. These steels have superior mechanical properties compared to conventional steels, making it possible to use smaller dimensions, be capable of lighter sections, and support higher loads. This, in turn, results in a significant reduction in carbon emissions **[1]**.

Ultra-High-Strength Steel (UHSS) has found numerous applications in the industry, including its use in automotive and aerospace components. Recently, researchers have been exploring the replacement of conventional steels with UHSS in structural elements in civil construction **[2]**. As structural elements, one potential application of these materials is in columns, where high load-bearing capacity is essential and achieving high ductility is not necessarily required **[3]**.

However, the use of this material also presents disadvantages. With the adoption of thinner sections, buckling, which is more dependent on geometry than on material strength, can become an essential factor to consider in the design of columns [1]. Furthermore, due to the sensitivity of steels to high temperatures, the response of UHSS in such conditions must also be regarded as one of the primary design considerations for steel structures [3].

1.2- Research objectives

When dealing with exceptionally strong steels, factors like the size of the elements, their connections, and the slenderness and strength-to-weight ratio of the

structure offer significant benefits in selecting the appropriate solution for each situation. In this way, research has sought to evaluate, specifically, ultra-high strength steel columns, in order to ascertain the behaviour of this type of structure, varying cross-sections, dimensions, load-bearing capacity and even the conditions of the environment in which the structure is inserted (as the example of this study).

The design specifications defined by technical standards were developed considering a yield strength limit for steel. The European standard (EN 1993-1-1:2005 **[4]** and EN 1993-1-12 **[5]**), for example, can be applied to the design of steel structures with a nominal yield strength of up to 700 MPa. On the other hand, the American Institute of Steel Construction (AISC 360-10) **[6]**, considers steels with a yield strength of up to 690 MPa. The Brazilian standard (NBR 8800:2008) **[7]**, considers steels with a yield strength of up to 450 MPa, and finally, the Chinese steel structure design code (GB50017-2003) **[8]** up to a steel grade of 420 MPa. However, compared to their previous editions, almost all of them have simply adopted the original design method based on traditional research into strength steel structures, meaning that more research and theoretical groundwork are still needed **[9]**. Therefore, to date, the design methods for high- and ultra-high-strength steel structures are not sufficiently mature.

Through the synergy of theory and simulation, this research aims to advance knowledge in structural fire engineering, ultimately contributing to the development of safer and more resilient built environments, by verifying the UHSS columns under fire conditions behaviour, using the parameters included in Eurocode as a base for analysis.

1-3- Outline of the thesis

This study is organised into five chapters. The first chapter (introduction) presents a brief overview of the use of Ultra-High-Strength Steel (UHSS) in buildings and some of the reasons why it is used and studied. This section also presents the structure of this thesis.

The second chapter is made up of a literature review that looks at what factors are taken into account when using this type of steel in building structures. This chapter also presents the differences between Ultra-High-Strength Steel and conventional (mild) steel and resumes previous studies investigations, material properties and how it works under fire, including experimental tests, finite element analysis and analytical models.

The third chapter focuses on the methodology used in this work. It begins by

presenting the experimental tests developed by Farmani et al. **[3]**, as well as the variables and parameters used throughout the analysis. The numerical model and the design equations and properties used for all the simulations are presented.

The fourth chapter presents the results and discussion, comparing the numerical results with the experimental results **[3]**, and shows the results developed for different heating rates (ISO 834 and Hydrocarbon), presented in the Eurocode EN 1991-1-2.

The last chapter (fifth) presents a brief conclusion from this work and other future investigations.

2- LITERATURE REVIEW

This chapter reviews the available research literature on the structural behaviour of Ultra-High-Strength Steel (UHSS) under fire.

This literature review aims to explore experimental tests and numerical models to improve understanding of the phenomena that occur in steel structures containing this type of material under fire conditions. This study also aims to improve the performance buckling curves available in the standards, leading to a much more accurate method of designing structures. The fire resistance time and the critical temperature is also investigated, as well as the creation of knowledge about the behaviour of this material at elevated temperatures.

High-strength steel has two main differences from ordinary (mild) steel: the stress-strain curve and the distribution of residual stresses. The magnitudes of the residual stresses and their relationship to the yield strength of the steel, have a significant impact on the material's mechanical properties and, consequently, on the buckling behaviour of steel components **[9]**. Therefore, although a great deal of research has been done in the past on the behaviour of this type of material in different situations, there is a need to investigate the subject deeper so that the parameters analysed in each situation are even more assertive.

Since these materials can suffer different phenomena if exposed to extreme conditions, such as a fire, structural fire resistance is always a focus of attention when designing steel structures. In addition, it is equally important to accurately assess the degree of damage to steel structures after a fire, which also serves as the basis for repairing steel structures after a fire.

2.1- UHSS – Ultra-High Strength Steel

Different classifications of steel can be found in the literature, depending on their strength, application and mechanical properties. High-strength steels are classified by Nogueira **[10]** and Lajarin **[11]** as: High Strength Low Alloy (HSLA), Ultra-High Strength Steels (UHSS), and advanced Strength Steels (AHSS).

In the context of civil engineering, Shi et al. **[9]** call Ultra High Strength Steel (UHSS) structures those with a yield strength (f_y) of more than 690 MPa, and High Strength Steel (HSS) structures those with a yield strength of less than the same

magnitude. However, for comparison and information purposes, according to Nogueira **[10]** and Lajarin **[11]**, in the automotive industry, steels can be differentiated according to their strength value, as HSS those with yield strength (f_y) between 210 and 550 MPa and ultimate stress (f_u) between 270 and 700 MPa. UHSS are those with a yield strength (f_y) of more than 550 MPa and a limit strength (f_u) of more than 700 MPa. Finally, AHSS steels can overlap the yield strength (f_y) value ranges for HSS and UHSS steels.

2.2- Previous studies

The study of the properties and behaviour of steel materials at high temperatures plays a fundamental role in engineering. In applications that involve the possibility of adverse high-temperature situations, such as a steel column in a fire compartment, it is essential to understand how materials behave when exposed to such extreme conditions.

In this context, Ultra-High Strength Steel (UHSS) has emerged as an outstanding material due to its combination of superior mechanical strength to low weight ratio, and its growing use has led to a greater need for studies into the behaviour of this type of material under high temperature conditions.

In recent years, numerical simulations have become an essential tool for studying structural behaviour under extreme conditions, allowing for evaluating complex and extreme scenarios where experimental studies alone are not always possible. Using methods, such as finite element analysis, provides valuable information on the response of UHSS to heat, allowing for the optimisation of design strategies and the development of more precise safety guidelines. Usually, the finite element method is developed alongside experimental analysis, intending to compare and analyse the results proposed by the two methods, so that parametric studies can be created.

In this context, this section provides a brief review of previous studies on the application of UHSS and the factors that are influenced by it, as well as the possible effects on the behaviour of structures of this type at elevated temperatures.

Farmani and Heidarpour **[3]** address the current challenge of using Ultra-High Strength Steel (UHSS) in buildings due to a lack of appropriate design guidelines. The study introduces new design equations specifically tailored for Grade 1200 UHSS circular hollow section (CHS) columns when exposed to high-temperature fires. These equations are developed by conducting comprehensive computer simulations and real-world

experiments on UHSS tube samples. The study also considers the unique way UHSS behaves when subjected to high temperatures, including its thermal creep. Furthermore, the research explores how factors like column shape, heating rate, and the stiffness of surrounding structures affect the design equations. Ultimately, the results show that these equations can accurately predict column failure temperatures, making UHSS a promising option for structural applications in buildings.

Su et al. **[9]**, present an in-depth experimental and numerical investigation of the local buckling behaviour of welded I-sections made of Ultra-High Strength Steel (S960) under combined compression and bending moment around the principal axis. The experimental results were then compared to the numerical investigation to validate finite element models, and together, they were used to assess the applicability of the relevant design interaction curves as set out in the European code. In doing so, the evaluation revealed that the European code results are safe but have slightly conservative failure load predictions.

Azhari et al. **[13]** studied the tensile mechanical properties of UHSS tubes under fire and after cooling from fire temperatures of up to 800° C to room temperature (residual properties). It was shown that the strength of the UHSS tube starts to decline when exposed to fire temperatures above 300 °C, and it nearly disappears when tested at 800 °C. In addition, to investigate the effect of steel grade on the in-fire and post fire mechanical behaviour of steel materials, the stress-strain curves of Grade 800 (High Strength Steel – HSS) tube specimens were presented and compared with those obtained for grade 1200 (UHSS) tube, and, it can be seen that while the ultimate strength of the HSS specimen cooled from 800 °C to room temperature is reduced to approximately 66% of that of the virgin HSS specimen at room temperature, the corresponding reduction factor for the UHSS (Grade 1200) is 41%. Thus, regarding the residual properties of both grades, the UHSS loses its residual strength after being submitted to 300 ºC, while the HSS loses its residual strength after being submitted to 700 ºC. The UHSS increases its ductility after exposure to 500 ºC, while the HSS starts when exposed to 600 ºC. These results indicate the higher sensitivity of the UHSS to the temperature history of the material.

More studies have been published regarding material and structural behaviour, but these were considered the most relevant to this investigation.

3- METHODOLOGY

In the field of Ultra-High Strength Steel under fire conditions, the selection and application of models, verification of material properties and appropriate methodologies are fundamental to the accuracy and reliability of research results. This section investigates the intricate details of the theoretical models already studied, the parameters involving the properties of this type of material and the methodological approaches undertaken in this research, providing a comprehensive understanding of the research framework.

This research investigates the experimental work developed by Mohammad Amin Farmani and Amin Heidarpour **[3]**, in which the authors aimed to develop design equations for CHS (Circular Hollow Section) columns in Ultra-High-Strength Steel under transient fire conditions. The study was, therefore, based on the same parameters and considerations as the reference, namely the properties of the material studied, dimensions of the sample model used, as well as loads and heating rates.

3.1- Experimental Tests

The experimental tests were carried out on CHS tubes of direct-quenched Ultra-High-Strength Steel with a nominal yield strength of 1200 MPa. The material was produced by SSAB Steel Company. According to the manufacturer's datasheet **[14]**, the chemical composition of the UHSS CHS tubes used in the experiment is listed in **Table 1**. **Table 2** brings the chemical composition of a steel with yield strength of 230 - 300 MPa from the same facturer (SSAB Company) named Docol 500DP for comparison.

Table 1 – Chemical Composition of UHSS CHS tubes used by Farmani et al. **[14]**

Element	C	Si	Mn	P	S	Cr	Ni	Mo	B
Content [%wt]	0.230	0.800	1.700	0.025	0.015	1.500	1.000	0.500	0.005

Table 2 - Chemical composition of steel named Docol 500DP from SSAB Company. **[15]**

Element	C	Si	Mn	P	S	Al	Nb + Ti	Cr + Mo	B
Content [%wt]	0.08	0.400	1.800	0.025	0.010	0.015	0.100	0.500	0.005

As Farmani et al. [2] reported, **Figure 1** shows the stress-strain curve of the UHSS obtained from standard tensile tests performed at room temperature. For comparison, the room-temperature stress-strain curve of a Grade 250 MPa mild steel tube of the same diameter and thickness, tested by Javidan et al. in **[15]** is presented.

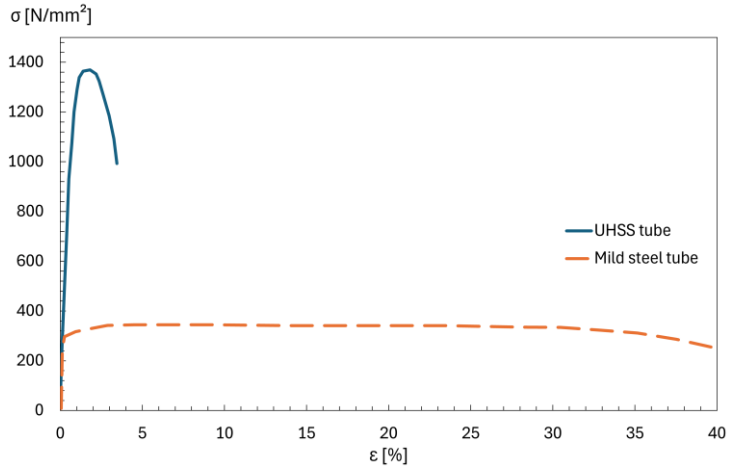

Figure 1 – Stress-strain curve of grade 1200 MPa CHS tube versus grade 250 mild steel tube at room-temperature.

One can see that the specimen made by UHSS is much stronger, but significantly less ductile than that of the mild steel tube. According to Azhari et al. **[16]**, this is justified by the martensitic microstructure of Ultra-High-Strength Steel, which is very strong but brittle.

Seven (7) same-sized UHSS CHS tube specimens were used for the study, all being tested under concentric axial compression. The UHSS CHS tubes with 780 mm length were used, with an external diameter of 76.1 mm and a wall thickness of 3.1 mm.

Figure 2 shows a 2D drawing presenting the general dimensions of the specimens. One specimen was used for room-temperature testing, and the six remaining were tested under non-standard fire conditions.

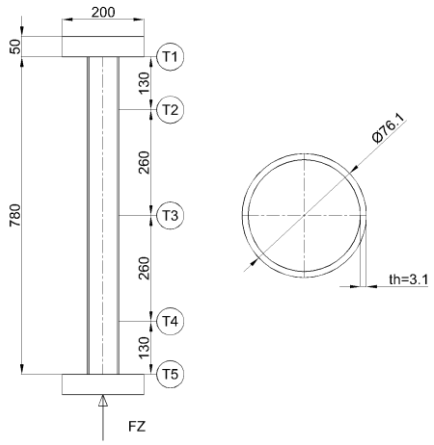

Figure 2 – Specimen general dimensions.

It is important to underline that geometric imperfections can directly affect the behaviour of columns under compressive loads. The initial imperfections were measured and implemented in the subsequent numerical simulations of the experiments. From the measurements, the maximum longitudinal imperfection is less than 0.5 mm for all specimens. Following AS 4100 **[17]** Australian Standard, any compressive member shall not deviate about its principal axis by an amount exceeding the greater of L/1000 and 3 mm, where L is the length of the element.

The test setup is presented in **Figure 3.** The compressive testing device has a big load capacity (5000 kN). The specimens were placed between two rigid plates. Linear Variable Differential Transformers (LVDTs) were used to measure the axial displacement, and also, 3 strain gauges were placed at the top, middle and bottom of the column to record the changes of axial strain over its length. Furthermore, a high-resolution 3D photogrammetry system called ARAMIS was used to monitor deformations over the specimen length.

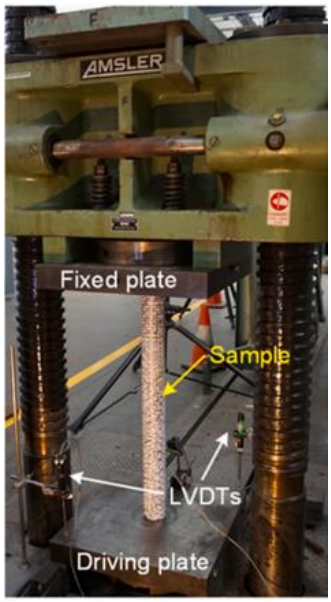

Figure 3 – Test setup of compressive test of UHSS CHS tubes. **[3]**

3.1.1- Room-temperature test

Figure 4a displays the load-displacement curve of the experiment at room-temperature. As seen, the load-bearing capacity was about 936 kN. **Figure 4b** shows the column failure mode and the principal strain distribution over its length. This measurement was developed by the ARAMIS software, representing a global buckling failure mode.

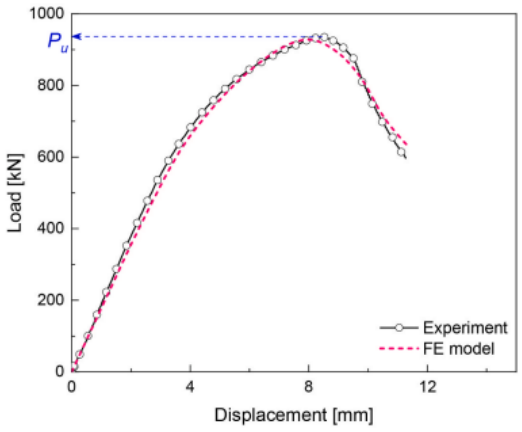

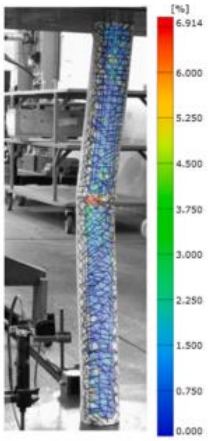

a) Load-displacement curve **b)** Failure mode and major strain distribution captured by ARAMIS software

Figure 4 – Compressive test of UHSS CHS tube at room temperature **[3].**

3.1.2- Fire tests

To experimentally investigate the behaviour of the UHSS under fire conditions, 6 tests were performed on specimens, using the gas furnace of Monash University - Structural Engineering laboratory. **Table 3** summarises the primary data from the experiments.

Table 3 - Test resume. **[3]**

Label[a]	Test variables			Test results
	Utilization factor, μ (–)	Load, P_0 (kN)	Nominal heating rate (°C/min)	Failure temperature, T_f (°C)[b]
U0.25-R20	0.25	234	20	641
U0.25-R5	0.25	234	5	617
U0.50-R20	0.50	468	20	553
U0.50-R5	0.50	468	5	522
U0.75-R20	0.75	702	20	454
U0.75-R5	0.75	702	5	431

[a] The general form of the label is "UX-RY", where X is the utilization factor, and Y is the heating rate in °C/min.

Three different load levels (μ) were used: 0.25 (25% of load-bearing capacity at room temperature), 0.50; and 0.75. Also, two (2) different heating rates were assumed: 20°C/min (R20) and 5°C/min (R5).

There is an inversely proportional relationship between the applied load and the failure temperature, which means that the lower the applied load, the higher the failure temperature and, consequently, the fire resistance time. The opposite occurs when it comes to the heating rate, where the higher the heating rate, the higher the element's failure temperature, however, the heating rate causes a much smaller change in the failure temperature when compared to the load level applied to the element. Following this logic, the scenario where the highest fire resistance is obtained, when it comes to the element failure temperature, is the combination of the lowest applied load and the highest heating rate, in this case the U0.25R20 specimen.

In order to analyse the temperature variation along the element, five (5) Type-N thermocouples were installed, identified by T1-T5 over the length of the element. **Figure**

5 represents the view of the gas furnace with a specimen ready to be tested.

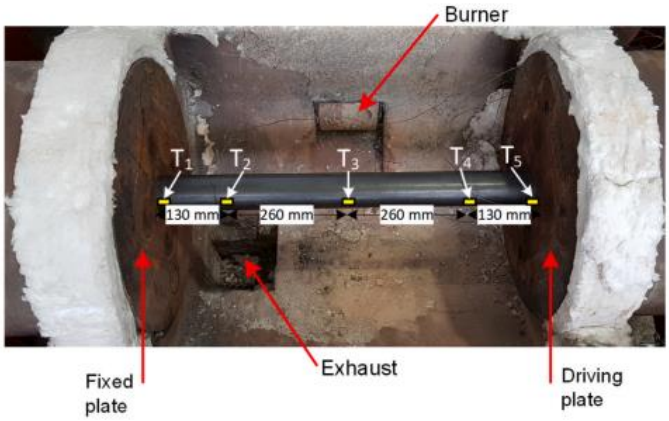

Figure 5 – Inside view of the furnace with a tube specimen ready to test and the location of thermocouples on the specimen. **[3]**

Figure 6 displays the evolution of the specimen temperature as measured by thermocouples T1-T5 in all 6 fire tests. As can be seen, the temperature at the mid-length (thermocouple T3) reaches the highest value. This may be justified by the position of the burner. The lowest temperature was determined for the positions T1 and T5, which correspond to the location near the end plates and the location of the exhaust. The thick base plates act as heat sinks for the specimen, justifying also the most minor temperature near T1 and T5.

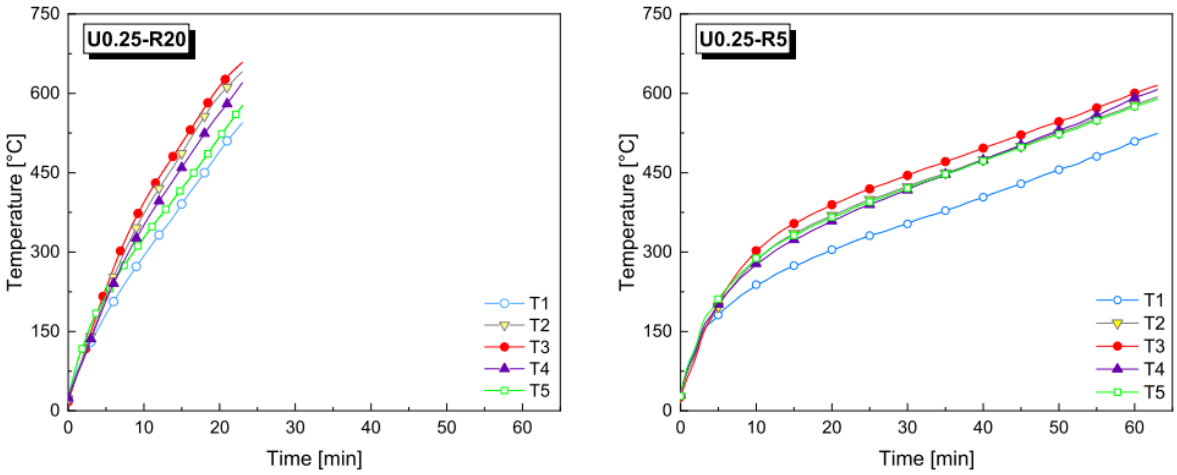

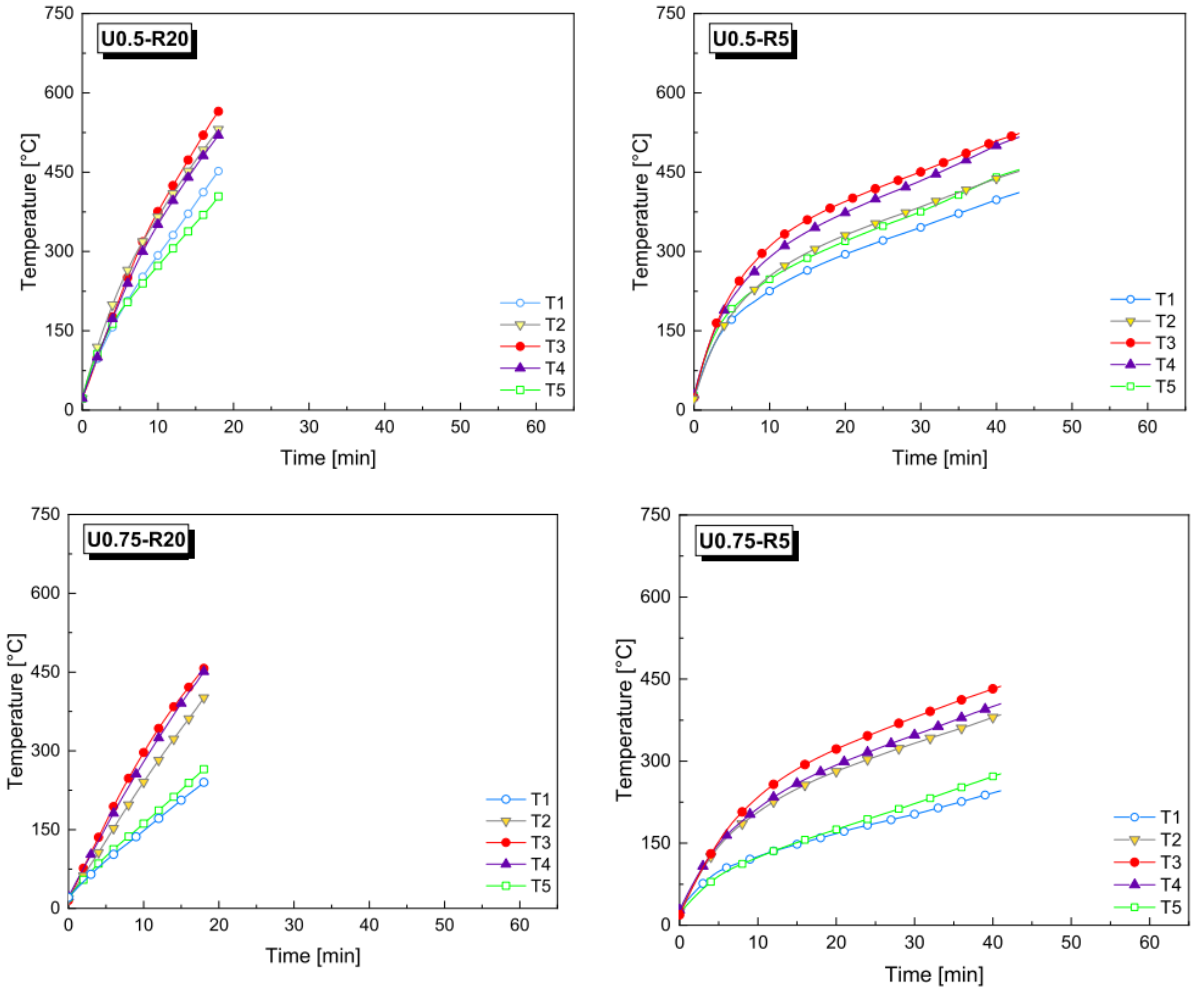

Figure 6 – Thermocouple readings x time – Fire tests. **[3]**

During each test, the displacement of the driving plate, which represents the axial deformation of the tube, was monitored. This data was recorded over time and correlated with the temperature along the mid-length of the tube (measured by the T3 thermocouple). **Figure 7** shows a meaningful comparison of the test results using 2 heating rates and 3 different load levels made by Farmani and Heidarpour **[3]**.

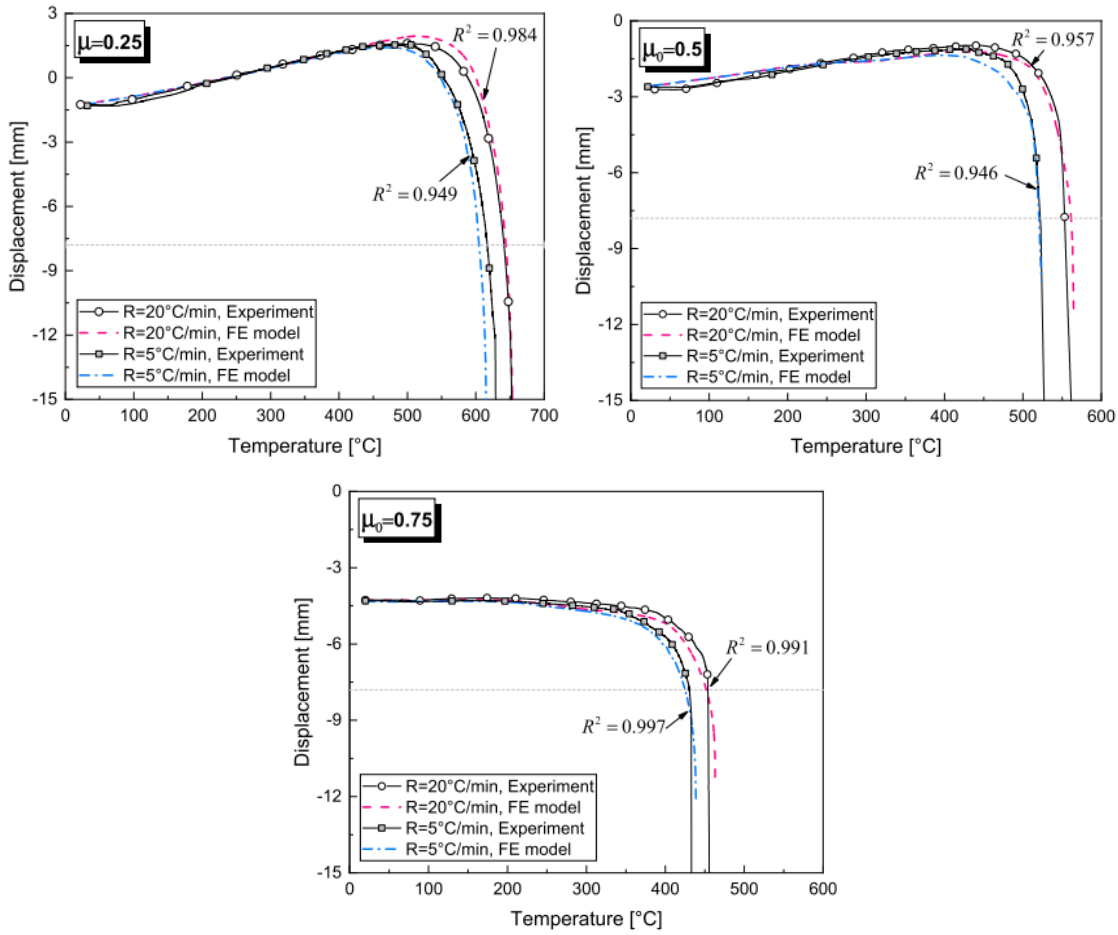

Figure 7 – Axial deformation vs. Temperature (at tube's mid-length) of UHSS – Fire tests. **[3]**

It is noted that a similar trend appears in all the displacement-temperature graphs, especially for the lower load levels. This indicates how the column responds to the combination of mechanical and thermal load to which it is being subjected during fire tests. These reactions develop in several stages, clearly represented in the diagram. A comprehensive analysis of the specimen behaviour under different conditions provides valuable information about its performance during fire conditions.

First, due to the compressive load applied, some initial contraction occurs, at room temperature. The higher the load level, the more initial axial contraction is installed in the column. As the process of heating initiates, an initial observation reveals that the column expands due to the thermal expansion properties of the material, keeping the load constant during the experiment. Nonetheless, as the temperature increases, a noteworthy phenomenon comes into play, where the mechanical shortening effect becomes more pronounced due to the decreasing of stiffness and strength of the Ultra-High Strength Steel (UHSS). Consequently, this phenomenon leads to a reduction in the expansion of

the column. The loss of stiffness and strength leads to the occurrence of buckling. Thereafter, the contraction accelerates, with an increasing displacement rate, until when the specimen can no longer support the axial load. This is when a sudden drop in the load applied occurs and the test terminates.

As shown in **Figure 8**, looking for the columns after the experiments, all of them had a fairly similar buckling failure mode. It is important to note that, the tests developed by Farmani and Heidarpour **[3]** describe the failure mode as being global, however, by analysing and interpreting the images, it is possible to interpret it differently, where the local failure mode becomes relevant. So, the failure mode can also be classified as being hybrid (local and global), and this was important for later analysing the imperfection modes used in the model, for validation of the numerical model.

Figure 8 – Failure mode of the UHSS tubes in the fire tests. **[3]**

According to European Standard EN 1363-1 **[18],** for the determination of fire resistance of structural elements, a column of length h in mm is deemed to have failed when its axial contraction reaches (C_{limit}) = $L/100$ mm, or its rate of axial contraction reaches $(dC/dt)_{limit}$ = $3L/100$ mm/min. In that study's case, the failure temperature was determined based on the first criterion, i.e., when the column contraction reached 7.8 mm.

As seen in **Table 3**, the higher the load level (μ), the lower the failure temperature (T_f). For example, at the same heating rate of 20°C/min., when the load level is μ= 0.25, the failure temperature is about 641°C. This failure temperature falls around 30% to 454 °C when μ= 0.75. On the other hand, the effect of the heating rate is so much less

significant than the load level. For all 3 load levels, when reducing the heating rate from 20°C/min to 5°C/min, leads to a decrease of around 4-6% in the UHSS column failure temperature.

3.2- Finite Element Analysis

In structural engineering, understanding the behaviour of materials under extreme conditions is fundamental to guaranteeing the safety and integrity of built environments. In particular, the performance of ultra-high strength steel (UHSS) columns under fire conditions is a critical area of research. This section investigates using numerical simulations, with ANSYS Mechanical APDL, to simulate the experiments performed on the UHSS columns at both room and fire temperatures, developed by Farmani and Heidarpour **[3]**.

This section uses computational analysis to model the complex interactions between UHSS materials and fire, shedding light on phenomena such as thermal expansion, material degradation and structural integrity under high temperatures. Taking advantage of the robust features of ANSYS Mechanical APDL, this study aims to provide information on the behaviour of UHSS columns under transient fire conditions, allowing us to understand what can happen to structural systems in fire-prone environments.

Finite element analysis in Ansys Mechanical APDL can essentially be divided into three main stages, according to Thompson **[19]**. Pre-processing: This phase involves modelling the geometry to be studied, selecting the element types, defining the material properties, generating the mesh, and applying the boundary conditions. The Solution: This includes defining the solution methods and subsequently developing the simulation. The Post-processing: This includes visualising, checking, printing and exporting the simulation results for analysis.

3.2.1- Finite elements

Considering that this study involves long columns with reduced thicknesses due to the use of UHSS, it was decided to use shell finite elements. These elements are ideal for structures where one dimension is significantly smaller than the other two. In the analyses carried out, two different types of shell finite elements were used: SHELL181 for mechanical analysis and SHELL131 for thermal analysis.

The SHELL 181 is a four-node 3D element with six degrees of freedom at each node: translations in the x, y, and z directions, and rotations about the x, y, and z-axes. This element has linear interpolation functions and full Gauss integration (2x2). Five Gauss points are used in the thickness. The top face is identified as LKEY 2, while the bottom face is identified as LKEY 1. This element has only been defined with one layer. **Figure 9** illustrates this element geometry **[20]**.

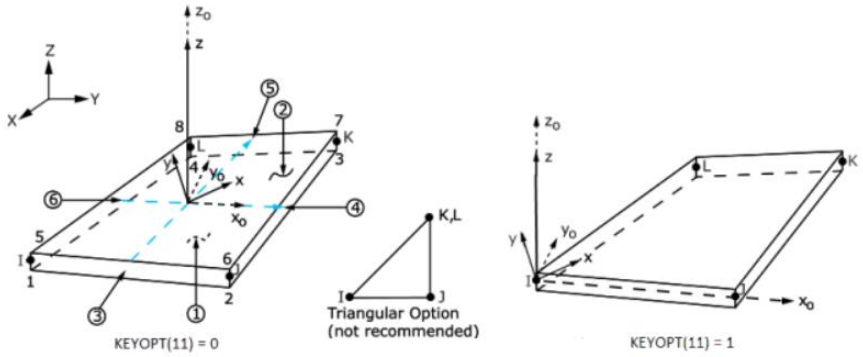

Figure 9 – SHELL181 finite element geometry. **[20]**

The SHELL131 is a 3D four-node element that can have up to 32 degrees of freedom per node, related to its nodal temperature, depending on the number of layers defined by the user. It uses linear interpolation functions with full Gauss integration (2x2). In this study, only one layer was considered, with linear temperature variation, due to the high conductivity of the materials used. The "PAINT" option was activated so that the temperature of the lower surface (BOTTOM), identified as LKEY 1, can be used in connection with the temperature of other types of finite elements. This setting is only relevant for the connection with solid elements, which only have one degree of freedom per node. **Figure 10** illustrates this element **[20]**.

Therefore, for this work, considering that there is only one layer, the element will have three degrees of freedom, corresponding to the temperatures TBOT, TE2 and TTOP.

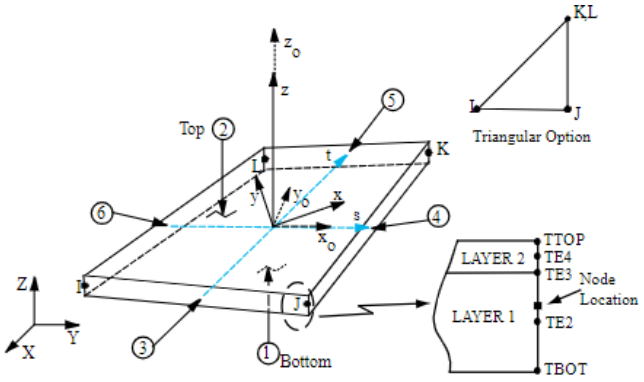

Figure 10 – SHELL131 finite element geometry. **[20]**

Depending on the application, convection and radiation can be applied to both sides of the surface defined by the element. So, in this case, the inner side of the tube will be represented by LKEY 1 (violet, bottom) and the outer side by LKEY 2 (green, top), as specified in **Figure 11.**

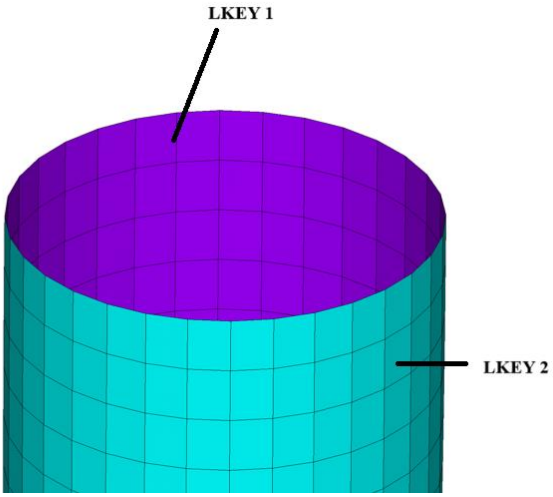

Figure 11 – Mesh on surface (internal and external).

3.2.2- Boundary Conditions and Mesh Configuration

The model includes the perfect contact between the column and the rigid plates to simulate the column boundary conditions more realistically. To this end, the fixed plate and the driving plate were modelled in the form of two blocks with dimensions of 200 mm × 200 mm × 50 mm, with a stiffness of 10 times that of the column (198 GPa), located symmetrically at both ends of the tube.

The support conditions for the FE model are illustrated in **Fig. 12 (a)**. As can be

seen, by restricting the degrees of freedom on the end plates, the top block was fully fixed, i.e. in all directions, while the bottom plate, which acted as the driving plate, could only move along the axis of the tube, in this case, the Z axis, where the compressive load is applied.

In this case, the column was divided into 80 divisions in the direction of its length and 16 around its diameter, totalling 2560 elements in the columns. When considering the elements of the plates for validation, the total number of elements is 3200 elements. The total number of nodes is 3202. The mesh is shown in **Fig. 12 (b)**.

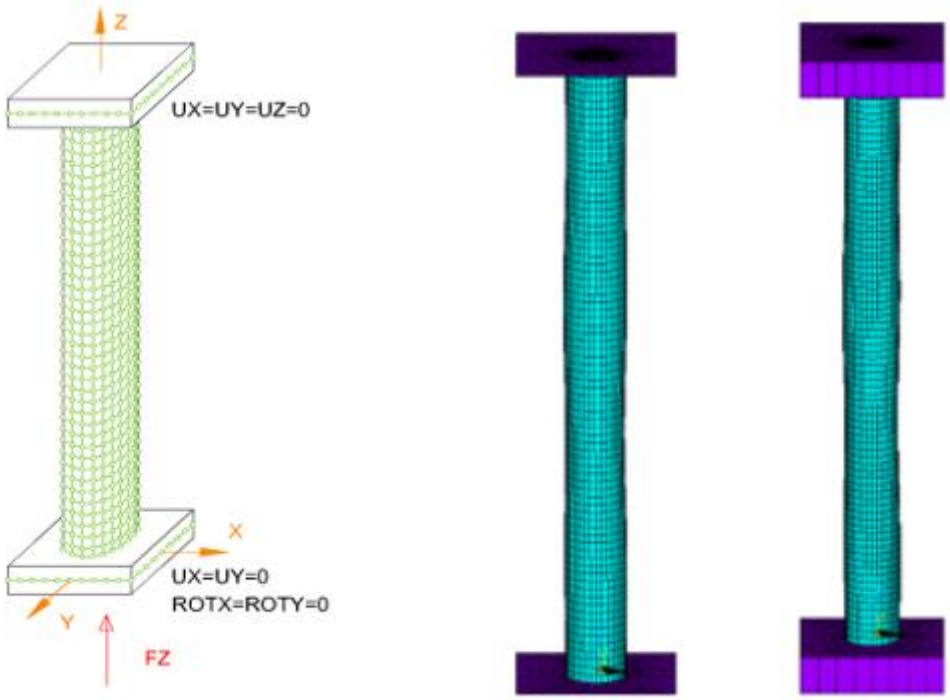

(a) **(b)**

Figure 12 – **(a)** Configuration of mesh, loading and boundary conditions. **(b)** Shell Element Modeling without and with shape.

Geometric imperfections can affect the behaviour of compressed members and should, therefore, be included in the finite element model. For this, a Linear Buckling Analysis was performed at room temperature and the column initial buckling modes were determined. Finally, initial global and local geometric imperfections were included into the model, as derived from eigenvalue buckling analysis, considering two instability modes, one global and one local. These modes were modified into imperfection modes, following the tolerances included in European Standards EN 10210-2 **[21]** and EN 10219-2 **[22]**, where, for global instability is adopted a tolerance of L/1000, in this case 0.78

mm, and for local instability, a tolerance of 2 % of the diameter is considered for circular hollow sections. In this case, the ratio D/t is 24.5, so the tolerance for local imperfection of 1.522 mm was considered. Those values were used to calculate the scale factor applied to update the position of the nodes. Geometrically and Materially Nonlinear Analysis with Imperfections (GMNIA) was selected to analyse the load-bearing capacity and thermo-mechanical analysis (fire resistance). **Figure 13** shows the tolerances of imperfection of the column studied.

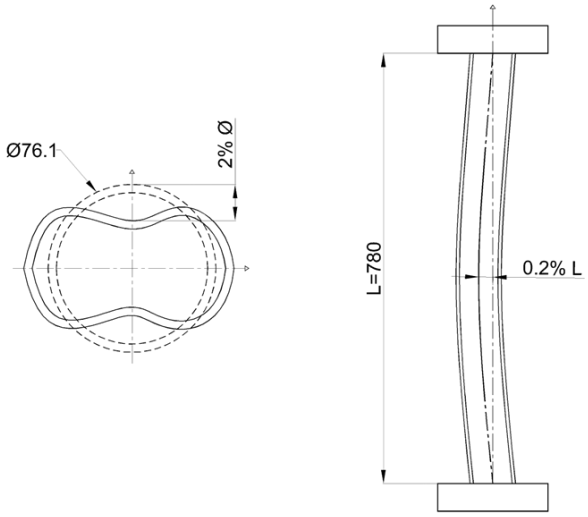

Figure 13 – CHS tolerances of imperfections - local and global.

An elastic buckling analysis of the element was then carried out, considering 10 modes of instability and separating modes 2 (for local instability) and 5 (for global instability) so that scale factors could be calculated to apply and consider both types of instability in the element. The **Figures 14** and **15** show the two modes used.

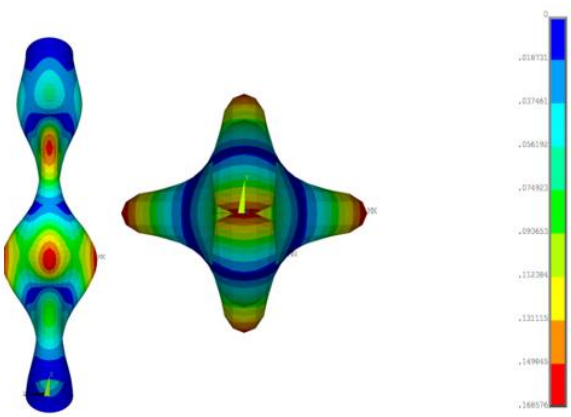

Figure 14 - mode 2 of instability – local.

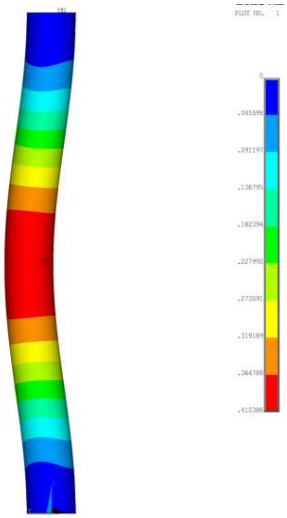

Figure 15 - mode 5 of instability – global.

3.2.3- GMNIA at room temperature

This is a computational method used in structural engineering to assess the performance of structures under fire, considering both geometric and material non-linearities along with imperfections. This approach is crucial for accurate predictions in structural behaviour, especially for the safety of critical applications such as bridges, buildings and other types of structures.

The aim here is to define the combination of the thermal load and the mechanical load, so that different load levels associated with different heating rates can subsequently be applied for analysis. The accuracy of this model is evaluated by the comparison with the experimental results.

The solution method used in this analysis was the arc length method, which is used to solve non-linear systems of equations, especially when the problem has one or more critical points. In terms of structural behaviour, a critical point is when the loaded element cannot withstand an increase in external forces, which means that the balance between internal and external forces is compromised, resulting in the instability of the structure **[23]**. In this case, the parameters included in the solution were defined by the incremental load (ΔF), and the minimum ($\Delta F_{mín.}$) and maximum ($\Delta F_{máx.}$) load increment.

$$\Delta F = 1000\ N$$

$$\Delta F_{mín.} = 1\ N \quad (R_{mín.} = 0.001)$$

$$\Delta F_{máx.} = 10\ 000\ N \quad (R_{máx.} = 10)$$

The convergence criteria adopted were based on force (F) and moment (M), both with a tolerance of 0.001 and a minimum reference value of 1 N and 1 N.m, respectively.

3.2.4- Nonlinear buckling analysis at high temperatures

For the tests including both mechanical and thermal loads, the temperature-dependent mechanical behaviour of the UHSS material should be included in the modelling. Following the constitutive law of the material, Ramberg Osgood modification (**Eq. 1**) was used to calculate the stress-strain curves of the material at different temperatures, based on the data table provided in Ref. **[3]**, shown in **Table 4**.

Table 4 – Parameters of the stress-strain relationship at room and elevated temperatures. **[3]**

T [ºC]	$k_{E,T}$	$k_{\sigma_{0.2,T}}$	$k_{\sigma_{1.5,T}}$	n_T	n'_T
20	1	1	1	5.62	6.55
100	0.9757	0.9292	0.9927	4.58	5.38
200	0.9265	0.8208	0.9462	4.56	4.62
300	0.8194	0.7333	0.8778	4.23	6.13
400	0.7388	0.6333	0.7564	3.31	4.18
500	0.6381	0.5042	0.5818	4.27	2.17
600	0.3558	0.2350	0.2720	4.39	1.64
700	0.1708	0.1083	0.1455	5.13	1.10
750	0.0957	0.0367	0.0487	5.65	4.07

$$\begin{aligned} \varepsilon_{(\sigma,T)} &= \sigma/E_T + 0.002\left(\sigma/\sigma_{0.2,T}\right)^{n_T} && \sigma \le \sigma_{0.2,T} \\ \varepsilon_{(\sigma,T)} &= (\sigma - \sigma_{0.2,T})/E_{0.2,T} + \left(0.015 - \varepsilon_{t0.2,T} - \left(\sigma_{t1.5,T} - \sigma_{0.2,T}\right)/E_{0.2,T}\right) \\ &\quad \times \left(\left(\sigma - \sigma_{0.2,T}\right)/\left(\sigma_{t1.5,T} - \sigma_{0.2,T}\right)\right)^{n'_T} + \varepsilon_{t0.2,T} && \sigma > \sigma_{0.2,T} \end{aligned} \quad \textbf{(1)}$$

Where:

$$E_{0.2,T} = \frac{E_T}{1 + 0.002 n_T \frac{E_T}{\sigma_{0.2,T}}} \quad \textbf{(2)}$$

Figure 16 represents the stress-strain curves obtained for the material at room and

elevated temperatures (up to 750 ºC), assuming the critical temperature is below this value.

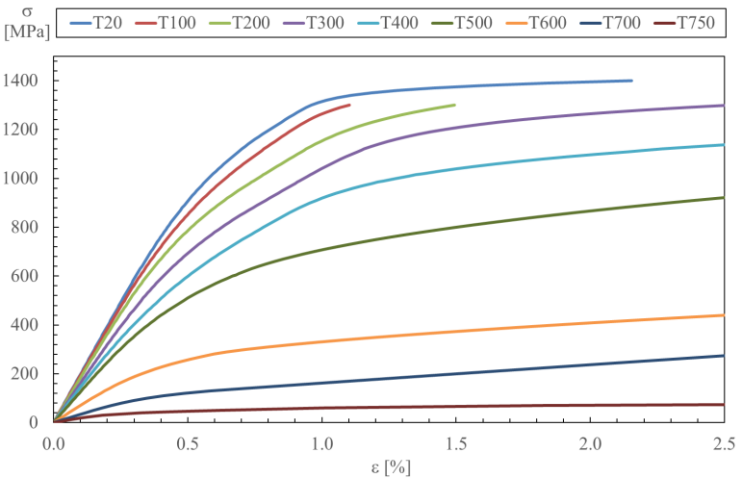

Figure 16 – Stress-strain curves of the UHSS from 20 º C to 750 º C.

In addition, the thermal elongation of the UHSS was also included in the model. This property was defined based on the EN 1993 1-2 **[24]**, that **Eq. 3** and **Figure 17** shows:

$$\begin{aligned} 20\,°C \le \theta_a < 750\,°C \quad & \frac{\Delta l}{l} = 1.2\times10^{-5}\theta_a + 0.4\times10^{-8}\,{\theta_a}^2 - 2.416\times10^{-4} \\ 750\,°C \le \theta_a < 860\,°C \quad & \frac{\Delta l}{l} = 1.1\times10^{-2} \\ 860\,°C \le \theta_a < 1200\,°C: \quad & \frac{\Delta l}{l} = 2\times10^{-5}\theta_a + 6.2\times10^{-3} \end{aligned} \qquad \textbf{(3)}$$

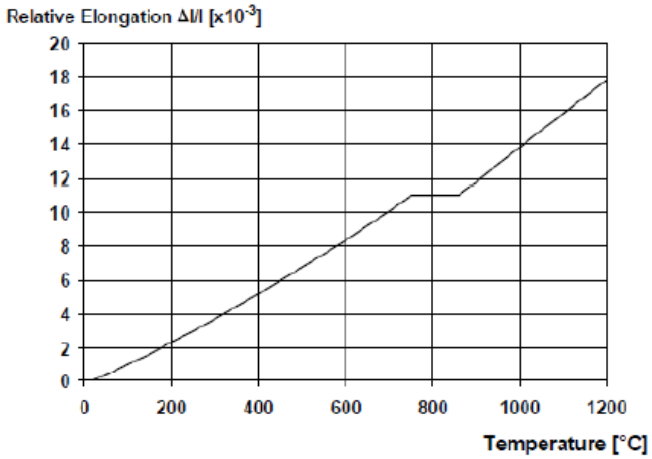

Figure 17 – Thermal elongation graph for elevated temperatures. **[24]**

For the temperature measurements, the arithmetic average of the readings from the five thermocouples during the experimental test (shown in **Fig. 6**) at a given time was calculated. A table of average temperature as a function of time was established for every specimen, allowing for the most accurate representation of the temperature variation inside the experimental test furnace. It is important to note that a reference temperature of 20 ºC was set as the initial condition for null deformation.

For the mechanical load, a new table is defined (**Table 5**), where t_{sim} corresponds to the expected end time of the simulation, and F_z represents the force in Newton applied in each case. This method was used to define the constant application of force over time, enabling the simulation to first demonstrate the deformation caused by the load on the element, similar to what occurs in the experimental test, just before adding the effects of temperature on the material.

Table 5 - Mechanical load by table (model).

t [sec.]	F [N]
0	0
10	F_z
t_{sim}	F_z

The solution method is incremental and iterative, using the modified Newton-Raphson, with a variable time step of $\Delta t = 10\ sec$, with the possibility of reducing to $\Delta t_{mín.} = 0.0001\ sec$ and a maximum time step of $\Delta t_{máx.} = 10\ sec$. The convergence criteria adopted were based on force (F) and moment (M), both with a tolerance of 0.001 and a minimum reference value of 1 N and 1 N.m, respectively.

3.2.5- Thermal Analysis

This study uses two types of thermal analysis, one using the standard fire ISO 834 temperature curve **[25]** and another one using the hydrocarbon curve **[26]**.

3.2.5.1- Thermal properties

The initial step involved switching the model in ANSYS from structural to thermal analysis, converting the structural elements (SHELL81) to thermal elements

(SHELL131). It was essential to input all the thermal properties of the carbon steel, including emissivity, thermal conductivity, specific heat and density, at room temperature and elevated temperatures, according to EN 1993 1-2 **[24]**. These thermal properties are as follows.

Emissivity (ε_m): Eq. 4

$$\varepsilon_m = 0.7 \tag{4}$$

Thermal conductivity (λ_a): Eq. 5

$$\begin{aligned} 20\,°C \le \theta_a < 800\,°C: &\quad \lambda_a = 54 - 3.33 \times 10^{-2}\theta_a\ W/mK \\ 800\,°C \le \theta_a < 1200\,°C: &\quad \lambda_a = 27.3\ W/mK \end{aligned} \tag{5}$$

Figure 18 depicts the conductivity variation with temperature:

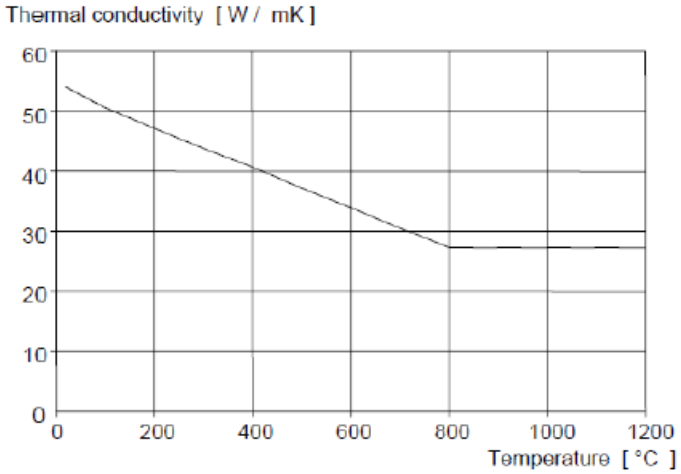

Figure 18 – Thermal conductivity of Steel – graph. **[24]**

Specific heat (c_a): Eq. 6

$$\begin{aligned} 20\,°C \le \theta_a < 600\,°C: &\quad c_a = 425 + 7.73 \times 10^{-1}\theta_a + 1{,}69 \times 10^{-3}{\theta_a}^2 \\ &\qquad + 2.22 \times 10^{-6}{\theta_a}^3\ J/kgK \\ 600\,°C \le \theta_a < 735\,°C: &\quad c_a = 666 + \frac{13002}{738 - \theta_a}\ J/kgK \\ 735\,°C \le \theta_a < 900\,°C: &\quad c_a = 545 + \frac{17820}{\theta_a - 731}\ J/kgK \\ 900\,°C \le \theta_a < 1200\,°C: &\quad c_a = 650\ J/kgK \end{aligned} \tag{6}$$

Figure 19 depicts the specific heat variation with temperature. The peak variation is related to the microstructure allotropic transformation from ferrite to austenite. This transformation is endothermic, which means that it is responsible for slowing down the rate of temperature increase.

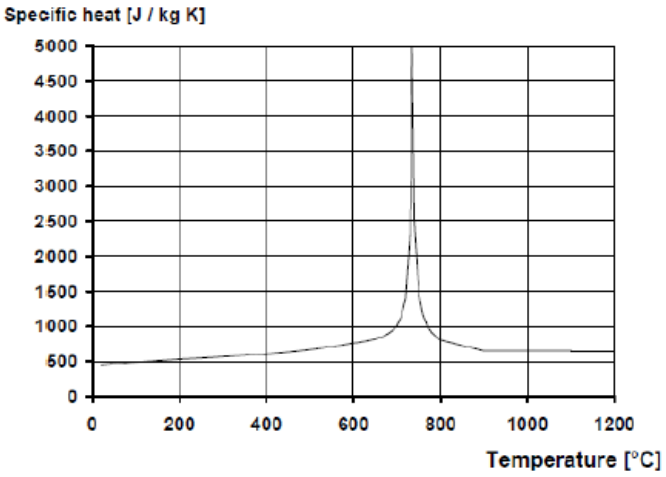

Figure 19 – Specific heat of Steel – graph. **[24]**

Density (ρ_a): Eq. (7).

$$\rho_a = 7850\ kg/m^3 \qquad \textbf{(7)}$$

It is important to note that the validation model accounted for the temperature applied to the nodes based on experimental data, reflecting the average temperature from the five thermocouples. The model also included convection and radiation effects on the outer surface of the tube, while the interior of the tube was treated as an adiabatic system.

3.2.5.2- The Standard fire ISO 834

To incorporate the ISO 834 **[25]** heating curve into the study, which represents the temperature variation used in standard fire tests, it was necessary first to conduct a thermal analysis to obtain the temperature profile of the column over time. This temperature field is then used in the subsequent thermo-mechanical analysis (constant mechanical load and incremental heating).

Following EN 1991 1-2 **[26]**, the Standard temperature-time curve is given by **Eq. 8**.

$$\theta_g = 20 + 345\ \log_{10}(8t + 1)\ [°C] \qquad \textbf{(8)}$$

Where θ_g is the gas temperature in the fire compartment in ºC, t is the time in minutes, and the coefficient of heat transfer by convection is $\alpha_c = 25\ W/m^2K$.

The **Figure 20** represents the temperature-time dependent curve for standard fire for 4 hours.

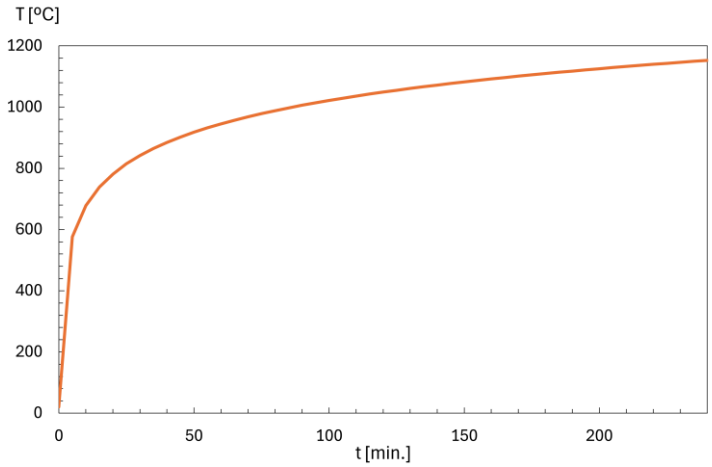

Figure 20 – Temperature-time curve for standard fire.

Subsequently, a node located outside the column was assigned to represent the furnace temperature, identified with "Enclosure 1". Following this, convection and radiation parameters were applied to the external surface of the column, and the initial temperature was set to 20°C.

To solve the thermal analysis, the heat transfer equation for an isotropic material can be expressed by **Eq. 9 [27]**.

$$\frac{\partial}{\partial x}\left(\lambda\frac{\partial\theta}{\partial x}\right) + \frac{\partial}{\partial y}\left(\lambda\frac{\partial\theta}{\partial y}\right) + \frac{\partial}{\partial z}\left(\lambda\frac{\partial\theta}{\partial z}\right) + Q = \rho \times C_p \times \frac{\partial\theta}{\partial t} \qquad \textbf{(9)}$$

Where Q is the heat generated within the body (disregarded in this case). The thermal conductivity is defined by λ, the density is defined by ρ, and the specific heat is

defined by C_p.

Eq. 9 is solved using the weighted residual method, which transforms the equation from its weak differential form to an integral form. The Galerkin approximation is also used to the approximation of the weighting function. The thermal solution is obtained incrementally and iteratively using the Newton-Raphson method, using the following time increments: $\Delta t = 60\ sec, \Delta t_{mín.} = 1\ sec,\ \Delta t_{máx.} = 60\ sec$.

The convergence criterion adopted was based on heat flow, with a tolerance of 0.001 and a minimum reference value of 1 W.

3.2.5.3- Hydrocarbon curve

As defined by EN 1991-1-2 **[26]**, the hydrocarbon fire curve represents a model for the temperature evolution in fires involving hydrocarbon-based fuels, such as oil products. Unlike standard fire curves, which are typically used for building materials, the hydrocarbon fire curve accounts for the more rapid temperature rise and higher peak temperatures characteristic of fires. This curve is essential for assessing the fire resistance of structures and materials exposed to such intense fire conditions, ensuring their safety and structural integrity in environments where hydrocarbon fires compartments are a significant risk. A few examples of these buildings are the petrochemical plants, offshore oil platforms, refineries, tunnels and even airports, among others.

The hydrocarbon temperature-time curve is given by **Eq. 10**.

$$\theta_g = 1080\ (1 - 0{,}325\ e^{-0{,}167t} - 0{,}675\ e^{-2{,}5t}) + 20\ \ [°C] \qquad \textbf{(10)}$$

Where θ_g is the gas temperature in the fire compartment in ºC, t is the time in minutes. The coefficient of heat transfer by convection is $\alpha_c = 50\ W/m^2K$.

Figure 21 represents the temperature-time dependent curve for hydrocarbons for 2 hours.

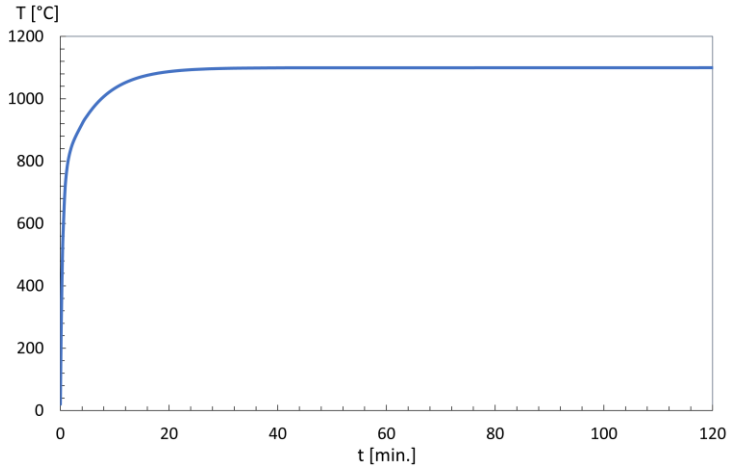

Figure 21 – Temperature-time curve for hydrocarbons – graph.

All the other parameters were maintained in the model. The solution to the simulation is obtained incrementally and iteratively using the Newton-Raphson method, with time increment $\Delta t = 10\ sec,\ \Delta t_{mín.} = 1\ sec, and\ \Delta t_{máx.} = 10\ sec$. The time is smaller due to the high heating rate of this fire curve. The convergence criteria adopted was based on heat flow, with a tolerance of 0.001 and a minimum reference value of 1 W.

3.2.6- Thermo-mechanical analysis

Using the temperature profile over time obtained from the thermal simulations, a nonlinear thermo-mechanical analysis was conducted. This process involved extracting the temperature values from the prior analysis using a command to read the files "*.rth" generated from the thermal solution. The command reads the thermal analysis results in 10-second increments. For intermediate values, a KBC variable is defined: when KBC equals 1, the intermediate temperature values remain constant until the next point is reached; when KBC equals 0, the intermediate values are determined by linear interpolation. It was also necessary to convert the element type from thermal to structural back. Additionally, the boundary conditions, forces, and integration points of the section had to be redefined, reverting to the conditions of the GMNIA (Geometrically and Materially non-linear imperfection analysis) analysis at high temperatures.

The solution method in this stage used time increments defined by the previously mentioned command. The convergence criterion adopted was based on displacement (U), with a tolerance of 0.001 and a minimum reference value of 3 meters, indicating that a

tolerance of 3 mm defines the determination of the element's equilibrium.

4- RESULTS AND DISCUSSION

This section presents the results derived from the simulations and analyses carried out, followed by a comprehensive interpretation of the results. This section aims to provide a clear and detailed description of the data generated, highlighting significant points of interest.

4.1- GMNIA at room temperature:

After carrying out the GMNIA analysis at room temperature, it was possible to compare the results obtained by Ansys with the experimental and numerical results presented by Farmani et al. **[3]**, as illustrated in **Figure 22**. In this figure 'C' represents the axial displacement at the central node of the driving plate (contraction), along the z-axis.

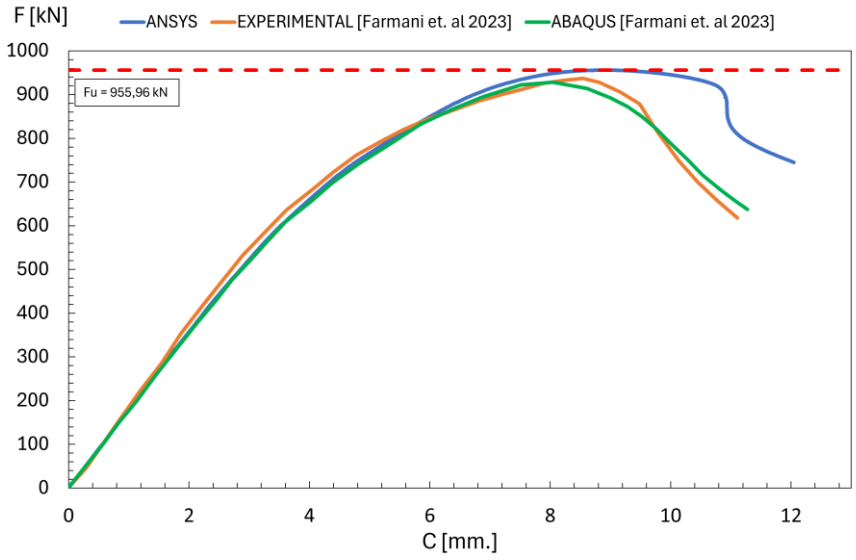

Figure 22 – GMNIA test at room temperature – comparison of results.

As can be seen, the simulation carried out in Ansys is in good agreement with the compared results, having only a difference in the final region of the curve. The maximum force obtained, which represents the load bearing of the column, was 955,96 kN, giving a relative error of 2,13 % compared to the experimental result and 3% when compared to the numerical model of the base article. It was also possible to compare the failure mode obtained in Ansys with the failure mode obtained experimentally in the experiment **[3]**,

as can be seen in **Figure 23**. This figure shows the deformations (1st principal mechanical strain) for the last moment of the simulation. The difference is related to the fact that a higher displacement was determined in the FE simulation, when compared to the experimental test.

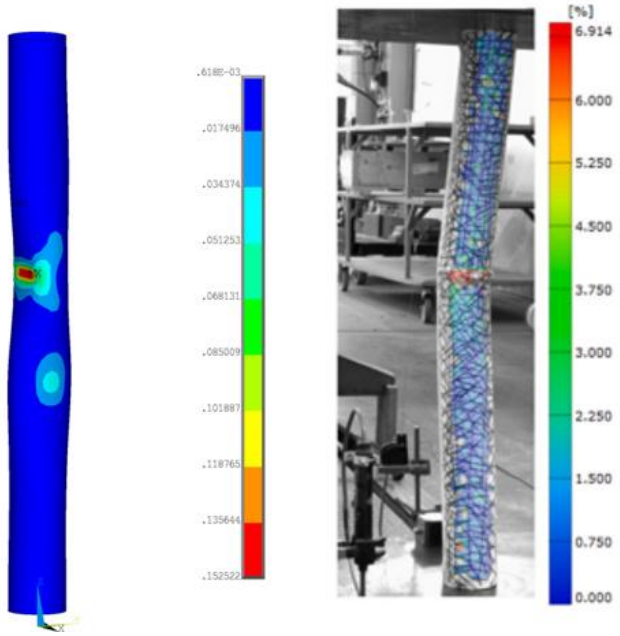

Figure 23 – Comparison of the failure mode of the UHSS column – Experimental **[3]** vs. FE model elaborated.

The model produced shows a more localized deformation of a greater degree than the experimental result. This is because the finite element model went further than the experimental one, due to the fact that the applied stress-strain curve took into account the mechanical properties of steel at a temperature of 20ºC calculated using the Ramberg-Osgood modification.

4.2- Elevated temperature validation

As previously mentioned, three distinct load levels (25%, 50% and 75%) and two heating rates (20ºC/min. and 5ºC/min.) were employed in this phase. The nomenclature for each simulation was assigned following the conventions of the experimental investigation, denoted as "UxRy" (where x represents the applied load level and y denotes the heating rate). Each of these simulations has been compared with the respective experimental and numerical results of the original investigation.

Figure 24 shows the results of the simulation including a constant load of 238990.5 N (representing 25% of the load level) and a heating rate of 20 ºC/min (R20). applied in the model and compare this with the experimental and numerical results developed by Farmani et al. **[3]**. This figure also shows is the evolution of the displacement rate (dC/dt), which in this case has been calculated as the moving average of a set of finite differences.

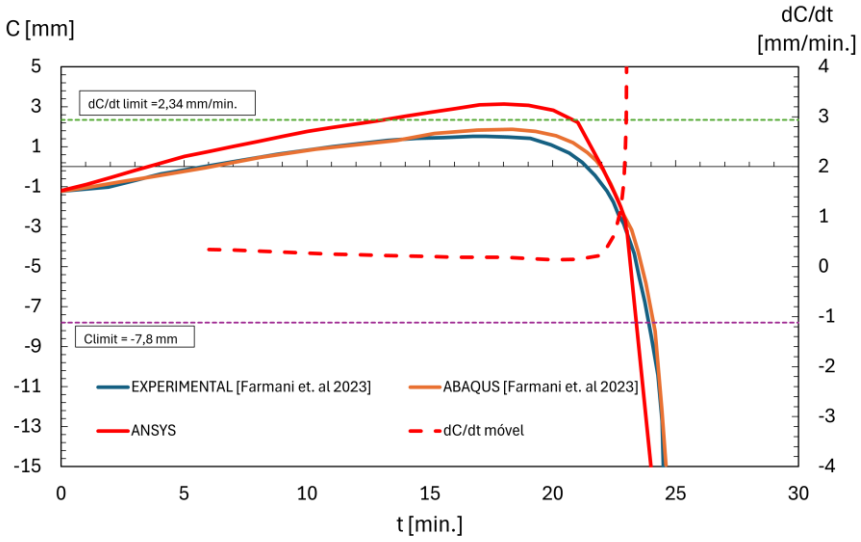

Figure 24 – U0.25R20 (25% of load bearing capacity with heating rate of 20 ºC/min.).

The results are consistent with the curves presented in the experimental investigation. Initially, the displacement is caused by the application of the mechanical load on the element. Over time, as the temperature increases, expansion is observed due to the effect of the temperature on the Ultra-High Strength Steel (UHSS). With the rising temperature, the stiffness and strength of the element decrease, and the displacement reverses and contraction prevails.

Figure 25 represents the body temperature of the element for the last time step of the simulation. The fire resistance time in this case was around 23 min, corresponding to a critical temperature of 619 ºC. **Figure 26** shows the Von Mises stress installed in the element at the last moment of the simulation.

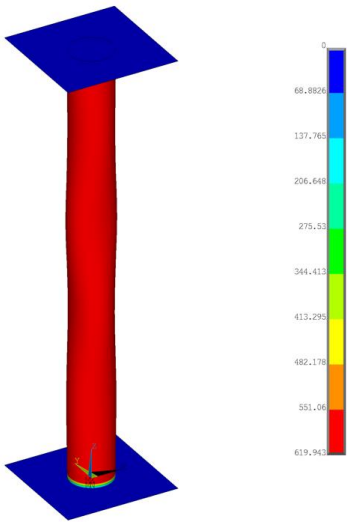

Figure 25 - Body temperature at the end of the simulation (last time step) – U0.25R20.

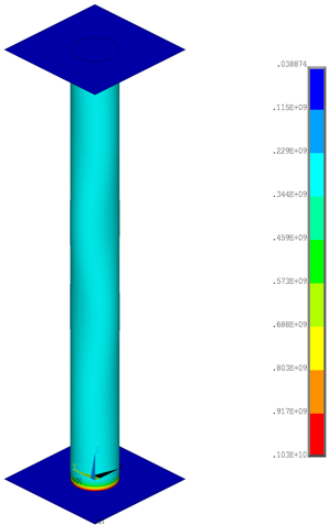

Figure 26 - Von Mises Stress at the end of the simulation (last time step) – U0.25R20.

The experimental test brings a value of 641 ºC for failure temperature but used a mechanical load of 234 kN. Therefore, it is considered a satisfactory result.

Figure 27 shows the results of the simulation including the same load level of 238990.5 N (25%) and a heating rate of 5 ºC/min (R5). The temperature is applied in the model over time. The displacement is compared with the experimental and numerical results obtained by Farmani et al. **[3]**.

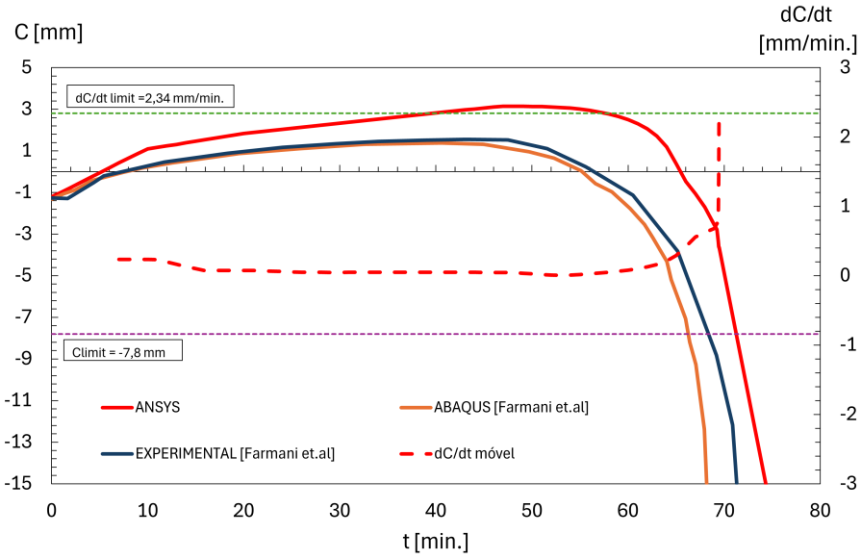

Figure 27 - U0.25R5 (25% of load-bearing capacity with a heating rate of 5 ºC/min.

Because the heating rate is lower than in the previous case, the fire resistance time

is significantly longer, around 69 minutes (2x more than the previous case). This is because, as the heating rate is lower, the column temperature takes longer to rise to the level where the stiffness and strength of the UHSS are lost. **Figure 28** represents the column's body temperature in the last simulation time, presenting 621 ºC. The failure temperature in the experimental test was 617 ºC. **Figure 29** shows the Von Mises stress installed in the element at the last moment of the simulation.

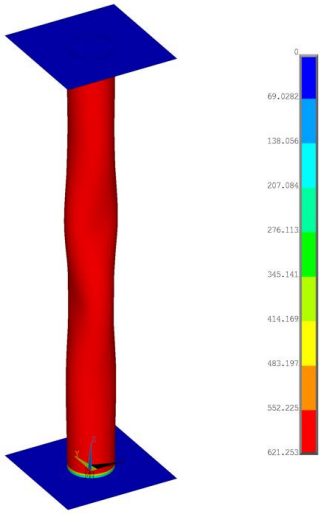

Figure 28 - Body temperature at the end of the simulation – U0.25R5.

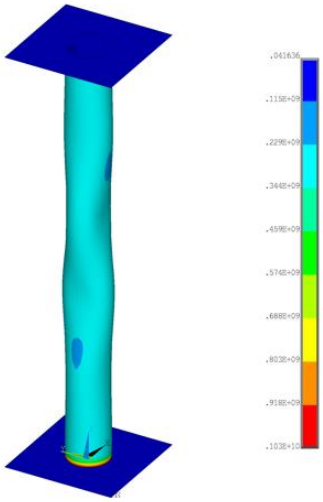

Figure 29 – Von Mises Stress at the end of the simulation (last time step) – U0.25R5.

Figure 30 shows the results of the simulation, including a compressive load of 477981 N (corresponding to 50% of the load-bearing) and a heating rate of 20 ºC/min (R20). The mechanical and thermal load is applied in the model and the results are compared with the experimental and numerical results presented by Farmani et al. **[3]**.

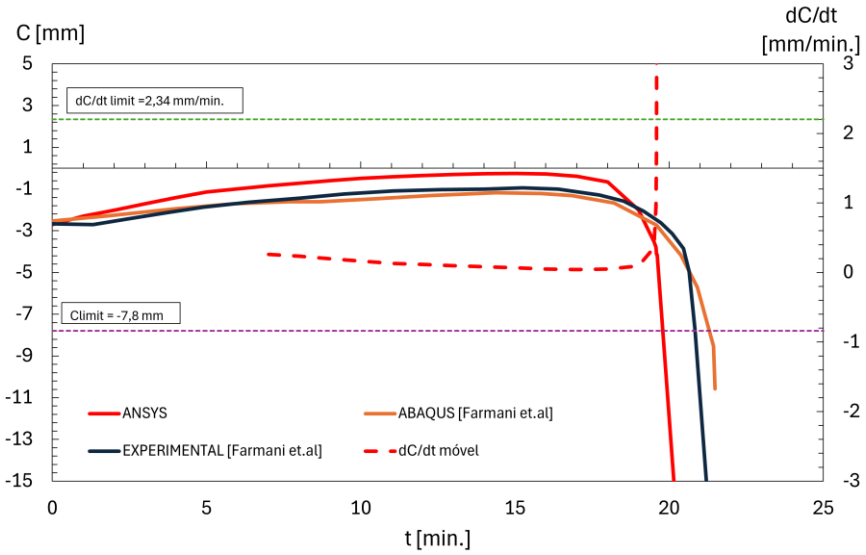

Figure 30 – U0.50R20 (50% of load bearing capacity with a heating rate of 20 ºC/min).

Compared to the first case, the difference can be seen in the application of the mechanical load, which is higher in this case. A reduction of approximately 17% in the fire resistance time of the column, when compared to the case with 25% of load level was verified. It shows that the heating rate is what interferes more actively with the behaviour of the structure in situations like this. The fire resistance time was around 19 minutes. **Figure 31** represents the body temperature of the column in the last time of the simulation, 527 ºC. This result should be compared with the failure temperature obtained in the experiment (553 ºC). **Figure 32** shows the Von Mises stress installed in the element at the last moment of the simulation.

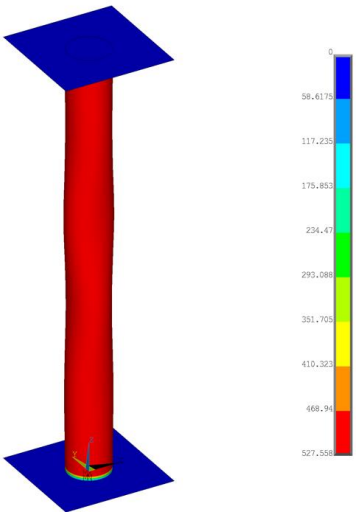

Figure 31 – Body temperature at the end of the simulation – U0.50R20.

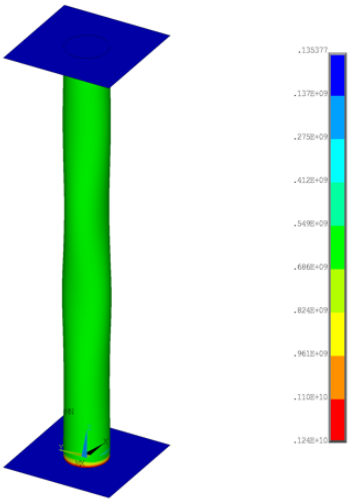

Figure 32 - Von Mises Stress at the end of the simulation (last time step) – U0.50R20.

Figure 33 shows the results of the simulation, including a compressive load of 477981 N (50%) and a heating rate of 5 ºC/min (R5), applied in the model. The vertical displacement (ANSYS) is compared with the experimental and numerical results of Farmani et al. **[3]**.

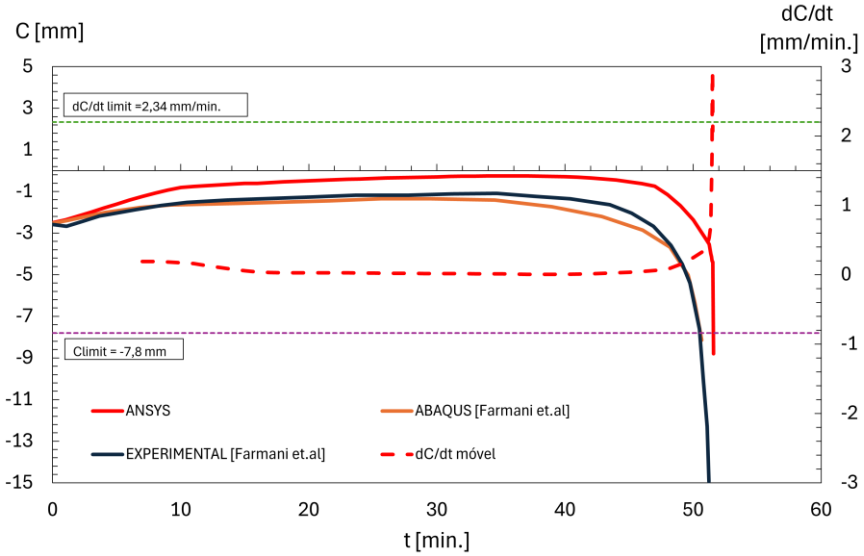

Figure 33 – U0.50R5 (50% of load bearing capacity with a heating rate of 5 ºC/min.).

In both cases with this level of load, the curves do not cross the positive displacement axis anymore. This means that although the element expands due to the initial deformation from the mechanical load, it doesn't expand enough to exceed the column original size at room temperature, unlike in the cases of load level with 25%. The

fire resistance time was around 51 minutes, corresponding to a reduction of approximately 26% when compared to the U0.25R5, with the same heating rate, but a lower load level. **Figure 34** represents the body temperature of the column in the last time step of the simulation, 527 ºC. The experimental failure time was 522 ºC. **Figure 35** shows the Von Mises stress installed in the element at the last moment of the simulation.

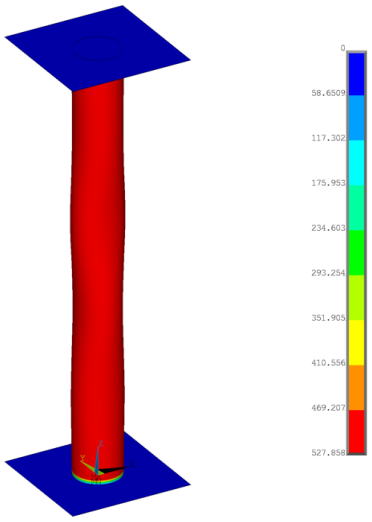

Figure 34 – Body temperature at the end of the simulation – U0.50R5.

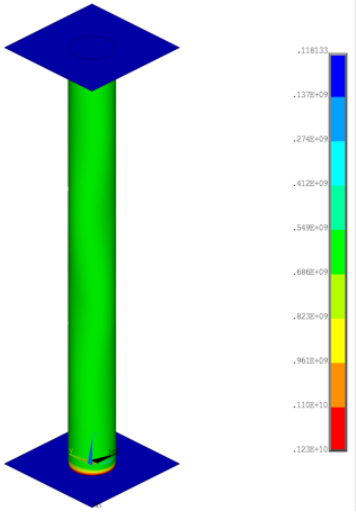

Figure 35 - Von Mises Stress at the end of the simulation (last time step) – U0.50R5.

Figure 36 shows the results of the simulation including a compressive load of 716971.5 N (corresponding to 75% load level) and a heating-rate of 20 ºC/min (R20). The constant mechanical and the variable thermal load were applied in the model, over time. The vertical displacement is compared with the experimental and numerical results presented by Farmani et al. **[3]**.

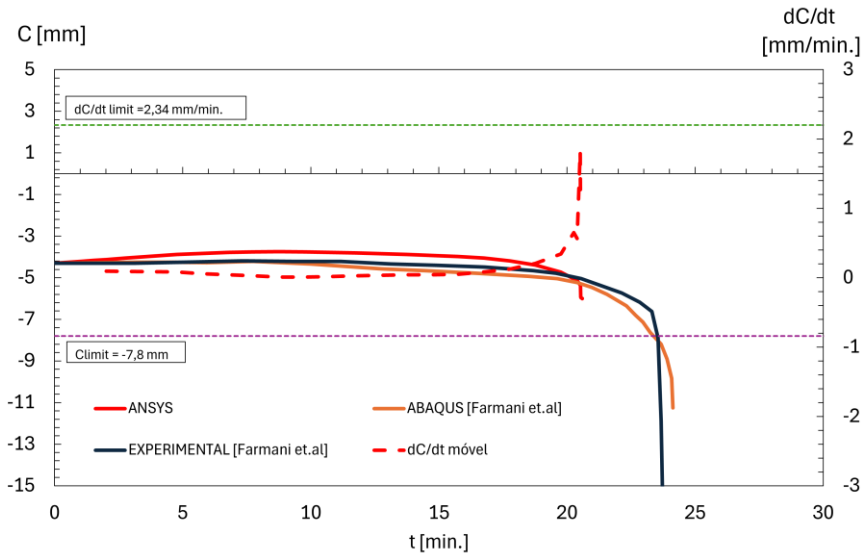

Figure 36 – U0.75R20 (75% of load bearing capacity with a heating rate of 20 ºC/min.).

In this case, the similarity in the behaviour of the curves towards the end of the simulation is reduced. The simulated fire resistance duration was approximately 20 minutes, with a failure temperature of 405 °C (**Figure 37**), as opposed to the 454°C reported in the aforementioned experimental investigation, which used a load of 702 kN, in the experimental test. This highlights a stronger influence of the mechanical load on the fire resistance. **Figure 38** shows the Von Mises stress installed in the element at the last moment of the simulation.

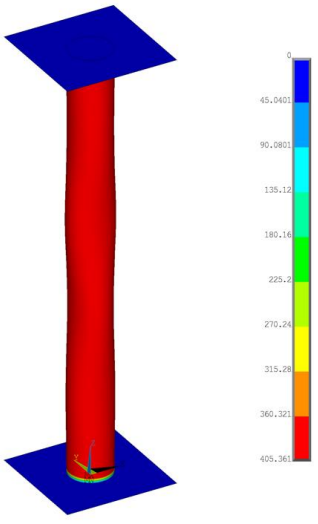

Figure 37 – Body temperature at the end of the simulation – U0.75R20.

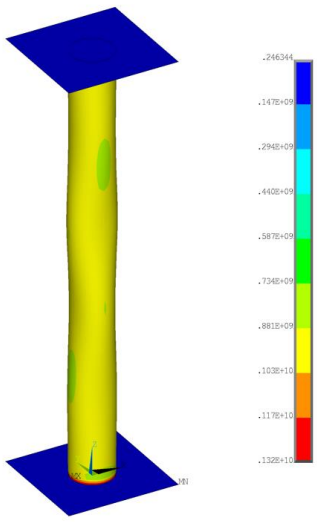

Figure 38 - Von Mises Stress at the end of the simulation (last time step) – U0.75R20.

Figure 39 shows the results of the simulation, including a compressive load of 716971.5 N (75%) and a heating rate of 5 ºC/min (R5). The results for the axial displacement are compared with the experimental and numerical results obtained by Farmani et al. **[3]**.

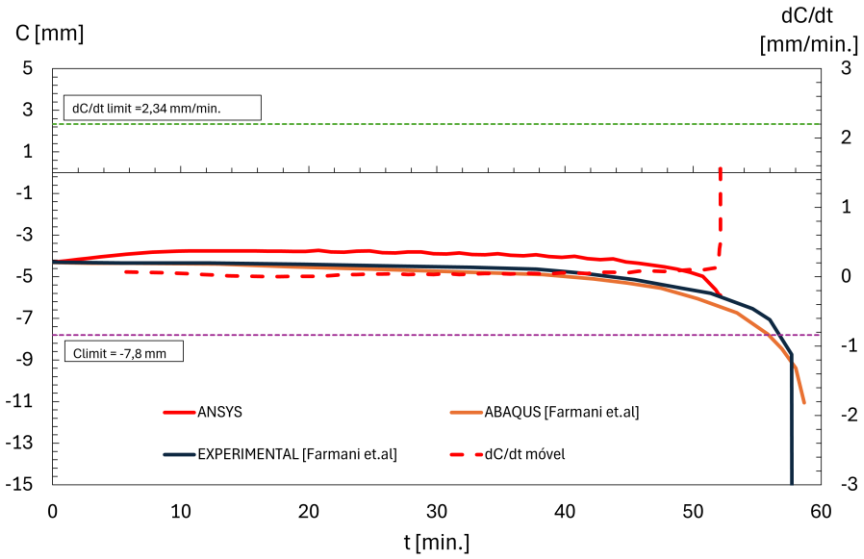

Figure 39 – U0.75R5 (75% of load bearing capacity with a heating rate of 5 ºC/min.).

The fire resistance time was approximately 52 minutes, with a failure temperature of 405 °C (**Figure 40**). The experimental failure temperature was 431°C. **Figure 41** shows the Von Mises stress installed in the element at the last moment of the simulation.

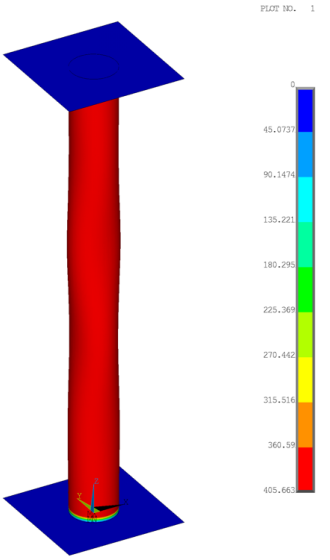

Figure 40 – Body temperature at the end of the simulation – U0.75R5.

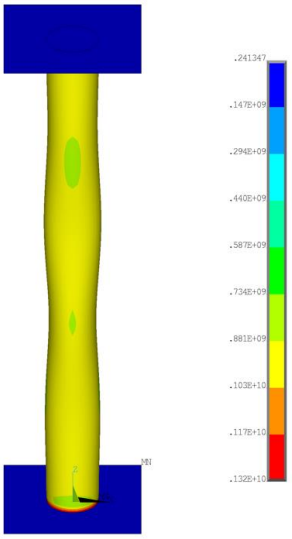

Figure 41 - Von Mises Stress at the end of the simulation (last time step) – U0.75R5.

Table 6 summarises the results obtained in Ansys and compares the failure temperatures obtained with those obtained from experiments.

Table 6 – Comparison of results between the study and the article by Farmani et al. **[3]**

NAME	LOAD ANSYS [kN]	LOAD ARTICLE (Experimental) [kN]	HEATING RATE [°C/min.]	FAILURE TEMPERATURE ANSYS [°C]	FAILURE TEMPERATURE (Experimental) [°C], [1]	RELATIVE ERROR	CRITICAL TIME [min.]
U0.25R20	238.99	234	20	619	641	-3.43 %	23
U0.25R5	238.99	234	5	621	617	0.64%	69
U0.50R20	477.98	468	20	527	553	-4.70%	19
U0.50R5	477.98	468	5	527	522	0.96%	51
U0.75R20	716.97	702	20	405	454	-10.79%	20
U0.75R5	716.97	702	5	405	431	-6.03%	52

The results of the simulations in Ansys are somewhat inconsistent with the data presented in the experimental investigation. For example, in the cases with load applied of 477.98 kN and 716.97 kN, despite the value of the heating rates (R5) or (R20), the failure temperature remained constant for the same load level, with only changing the critical time. Nevertheless, the failure temperatures showed relative errors that were considered to be within the accepted limits.

4.3- Thermal Analysis

As previously mentioned, this study includes two thermal simulations to analyse the behaviour of the UHSS column under different fire curves. This topic will present the results of the thermal simulations following the ISO 834 **[25]** (Standard fire test) and hydrocarbon curves.

4.3.1- Standard fire test

Figures 42 - 45 show the nodal temperature of the column under standard fire conditions for 30, 60, 90 and 120 min., respectively.

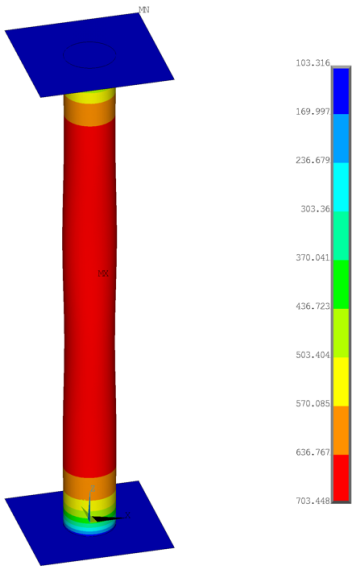

Figure 42 – Nodal temperature at 1800 seconds (30 min.) for Standard Fire test.

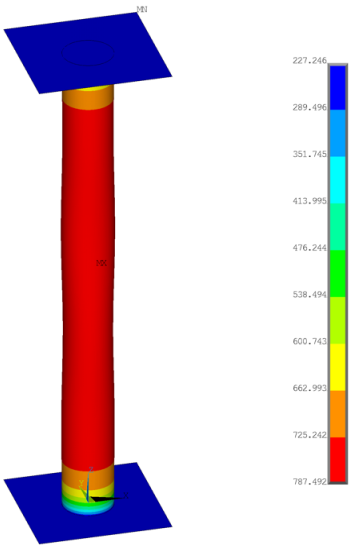

Figure 43 – Nodal temperature at 3600 seconds (60 min.) for Standard Fire test.

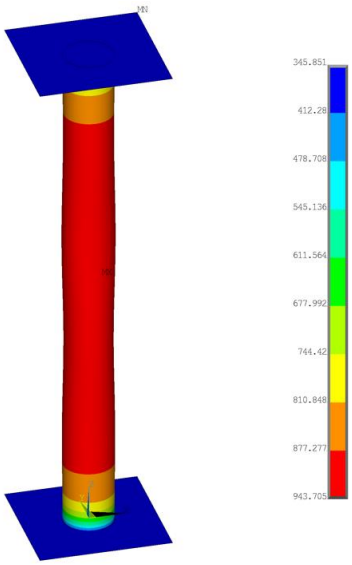

Figure 44 – Nodal temperature at 5400 seconds (90 min.) for Standard Fire test.

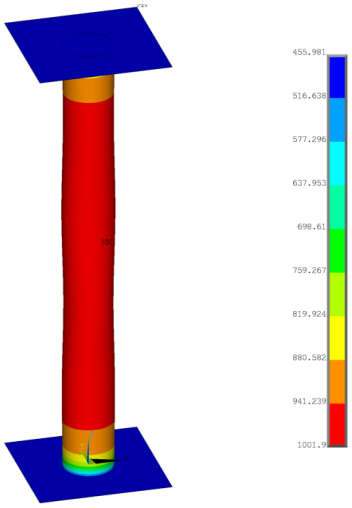

Figure 45 – Nodal temperature at 7200 seconds (120 min.) for Standard Fire test.

Figure 46 shows the graph representing the column's temperature-time evolution. The results are presented in the same locations as the thermocouples used in the experimental test. It is important to note that the curves representing thermocouples T1 and T5 and T2 and T4 respectively are superimposed on each other, because the model is symmetric, as depicted in **Figure 5**.

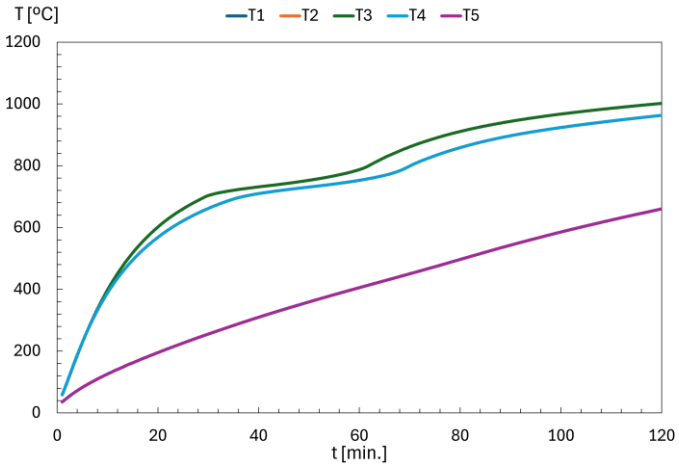

Figure 46 – Temperature-time behavior in thermocouples areas for Standard Fire test.

4.3.2- Hydrocarbon curve

Figures 47 - 52 show the nodal temperature of the column under hydrocarbon fire

conditions for 5, 10, 30, 60, 90 and 120 min.

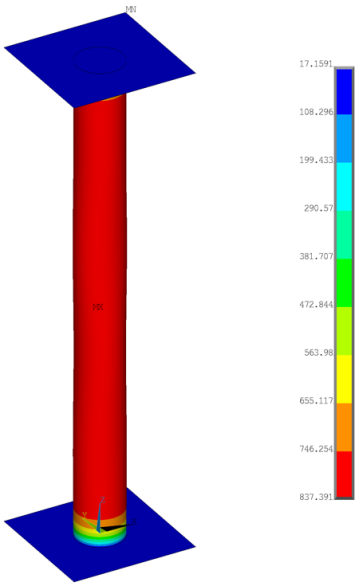

Figure 47 – Nodal temperature at 300 seconds (5 min.) for Hydrocarbon curve.

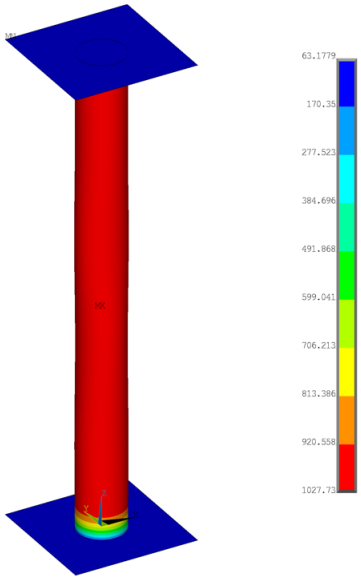

Figure 48 – Nodal temperature at 600 seconds (10 min.) for Hydrocarbon curve.

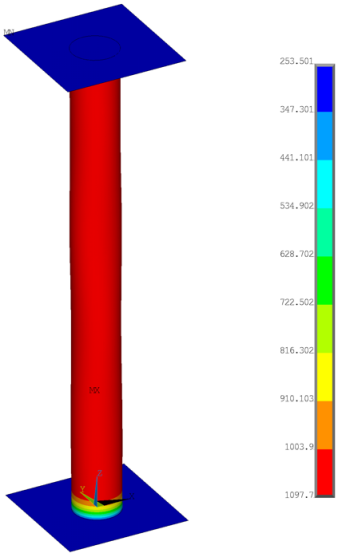

Figure 49 – Nodal temperature at 1800 seconds (30 min.) for Hydrocarbon curve.

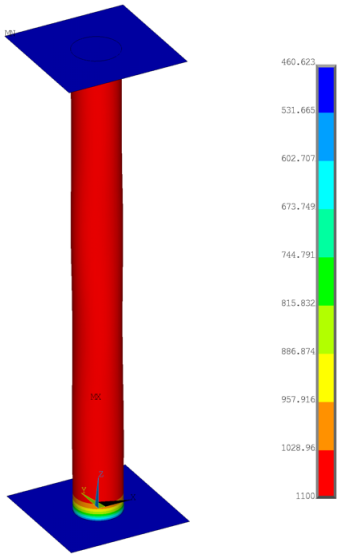

Figure 50 – Nodal temperature at 3600 seconds (60 min.) for Hydrocarbon.

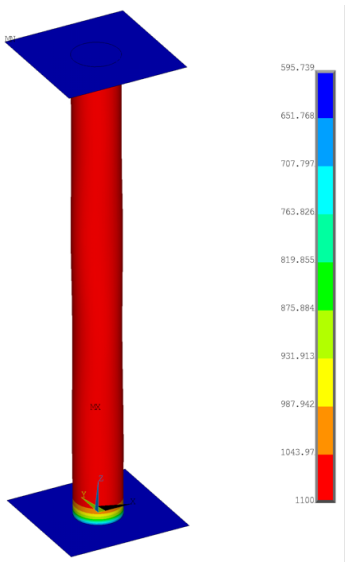

Figure 51 – Nodal temperature at 5400 seconds (90 min.) for Hydrocarbon curve.

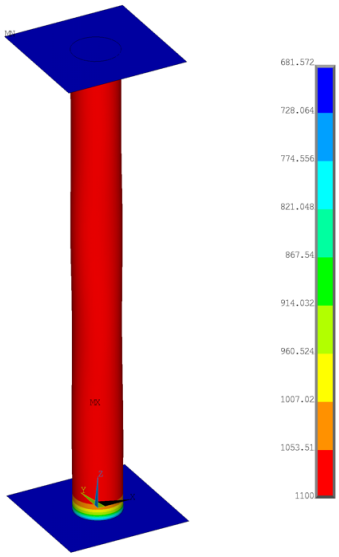

Figure 52 – Nodal temperature at 7200 seconds (120 min.) for Hydrocarbon curve.

The **Figure 53** shows the graph that represents the temperature-time evolution of the column, using the same nodal temperatures as used in the experimental tests. In this case, the curves corresponding to thermocouples T2, T3, and T4 overlap because they are situated in regions experiencing identical temperature variations (symmetry). Conversely, the curves for thermocouples T1 and T5 overlap at lower temperatures and exhibit a less pronounced temperature variation. This is explained by their proximity to the ends of the column (end plates), where the plates act as heat sinks. The graph also demonstrates a very high-temperature gradient near the end plates.

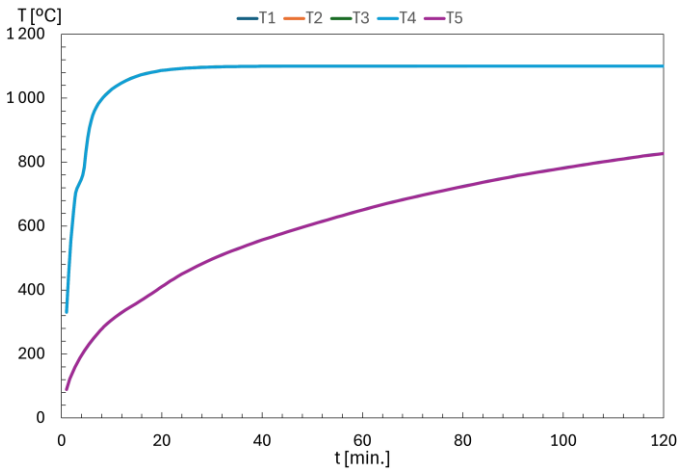

Figure 53 – Temperature-time behavior in thermocouples areas for Hydrocarbon curve test.

4.4- Thermo-mechanical analysis

At this stage, the objective is to combine the mechanical load with the thermal analysis models. Specifically, a load level (25%, 50%, or 75% of the load bearing capacity at room temperature) was applied to the central node of the bottom plate and the simulations were then repeated to determine the fire resistance time under varying temperature conditions as described by these curves. Subsequently, the column was classified following EN 13501-2 **[28]**, which gives the fire classification of construction products and building elements using data from fire resistance tests.

Figure 54 shows the displacement along the column length (z-axis) with the temperature varying according to the Standard Fire curve **[25]** and a mechanical load of 238990.5 N applied in the driving plate. The fire resistance time was around 21 minutes, with a failure temperature of 621 ºC, as depicted in **Figure 55**. According to EN 13501-2 **[28]**, the column exposed to these temperature and mechanical load conditions is classified as R20. **Figure 56** shows the Von Mises stress installed in the element at the last moment of the simulation.

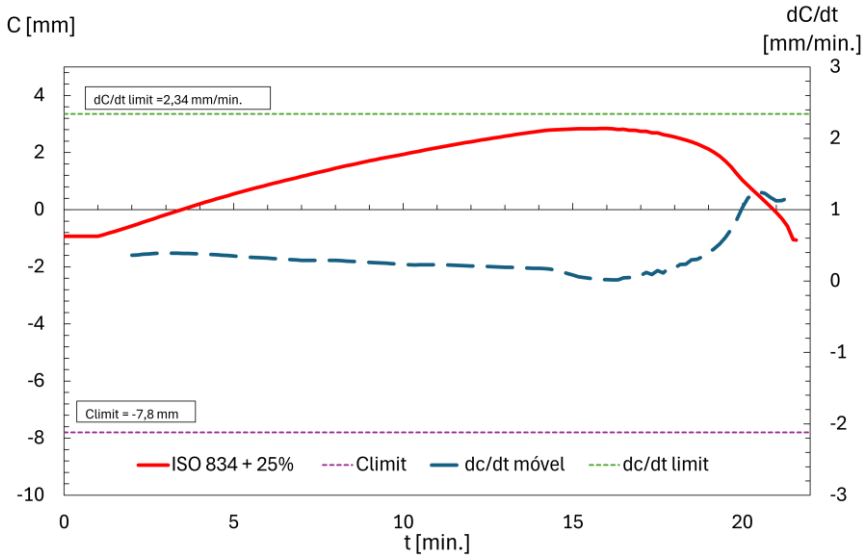

Figure 54 – Graph of displacement-time relationship for standard fire temperature + 25% of load bearing capacity at room temperature.

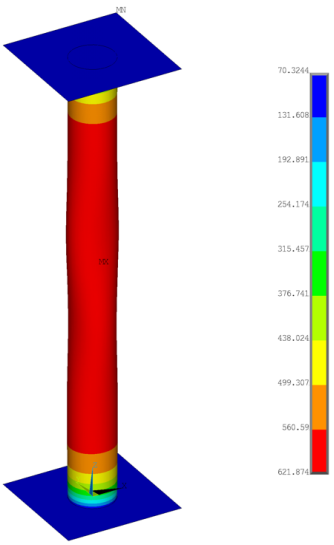

Figure 55 – Body temperature at the end of the simulation – ISO 834 **[25]** + 25%.

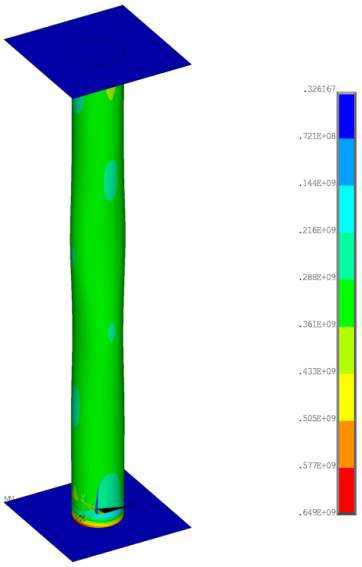

Figure 56 - Von Mises Stress at the end of the simulation (last time step) – ISO 834 **[25]** + 25%.

Figure 57 shows the displacement along the column length (z-axis) with the temperature varying according to the ISO834 standard curve **[25]** and a mechanical load of 477981 N applied in the driving plate. The fire resistance time was around 15 minutes, with a failure temperature of 527 ºC, as depicted in **Figure 58**. According to EN 13501-2 **[28]**, the column exposed to these temperature and mechanical load conditions is classified as R15. **Figure 59** shows the Von Mises stress installed in the element at the last moment of the simulation.

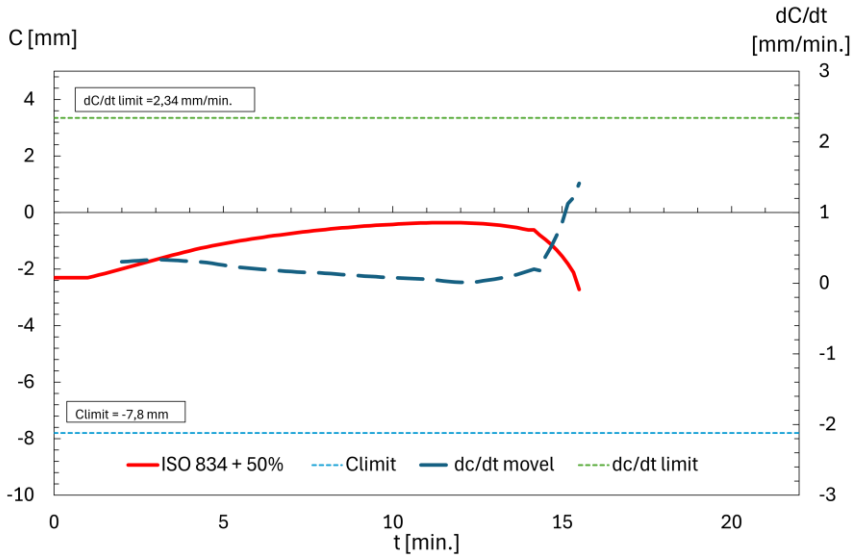

Figure 57 – Graph of displacement-time relationship for standard fire temperature + 50% of load bearing capacity at room temperature.

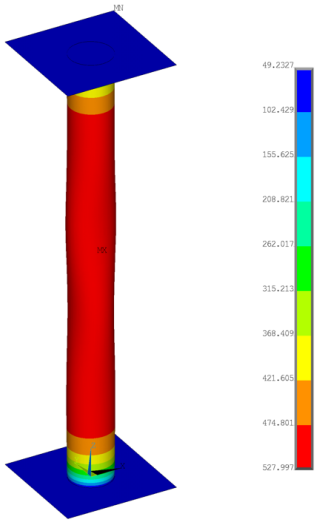

Figure 58 – Body temperature at the end of the simulation – ISO 834 **[25]** + 50%.

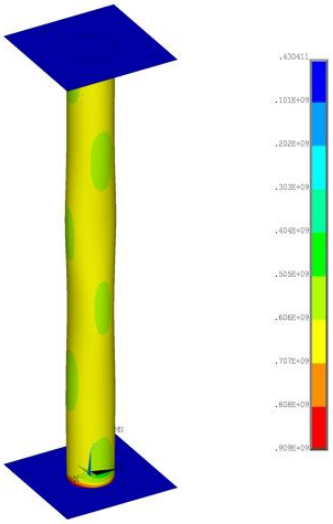

Figure 59 - Von Mises Stress at the end of the simulation (last time step) – ISO 834 [25] + 50%.

Figure 60 shows the displacement along the column length (z-axis) with the temperature varying according to the ISO834 curve **[25]** and a mechanical load of 716971.5 N applied in the driving plate. The fire resistance time was around 10 minutes, with a failure temperature of 403 ºC, as depicted in **Figure 61**. In this case, the column does not meet the standard's minimum requirement of 15 min (minimum fire rating class), this element cannot be classified under these conditions. It is essential to propose an insulation solution for the column to meet the minimum fire requirements. This would reduce its direct exposure, enabling it to withstand fire conditions under the specified temperature for longer time. **Figure 62** shows the Von Mises stress installed in the element at the last moment of the simulation.

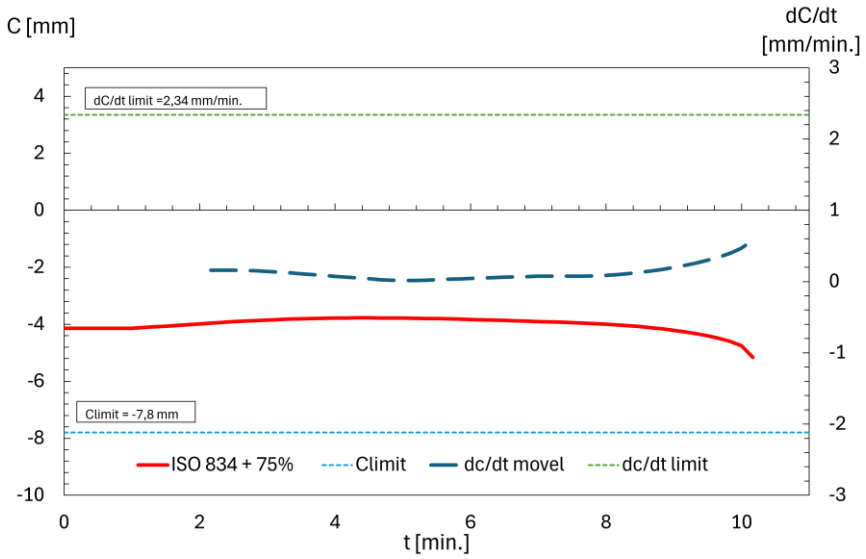

Figure 60 – Graph of displacement-time relationship for standard fire temperature + 75% of load bearing capacity at room temperature.

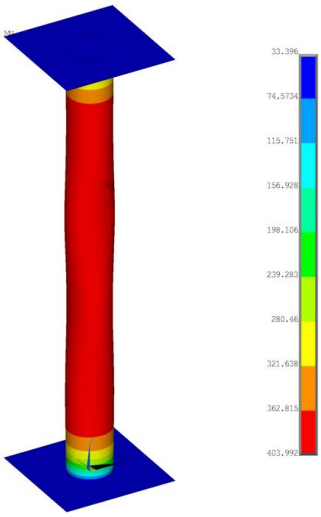

Figure 61 – Body temperature at the end of the simulation – ISO 834 **[25]** + 75%.

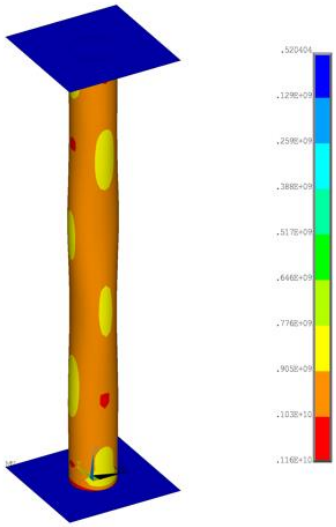

Figure 62 - Von Mises Stress at the end of the simulation (last time step) – ISO 834 [25] + 75%.

Figure 63 shows the displacement along the column length (z-axis) with the temperature varying according to the hydrocarbon curve **[26]** and a mechanical load of 238990.5 N applied in the driving plate. The fire resistance time is very small, around 2 minutes, with a failure temperature of 598 ºC, as depicted in **Figure 64**. **Figure 65** shows the Von Mises stress installed in the element at the last moment of the simulation.

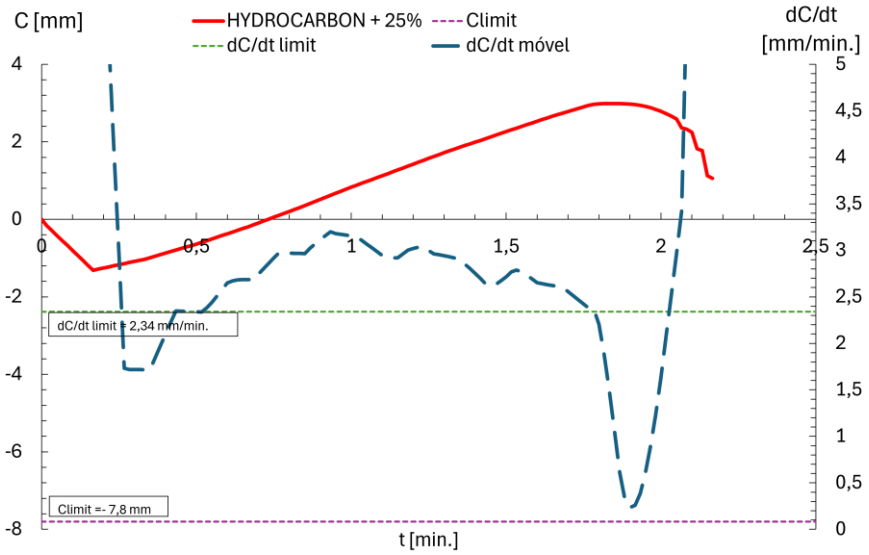

Figure 63 – Graph of displacement-time relationship for hydrocarbon fire curve + 25% of load bearing capacity at room temperature.

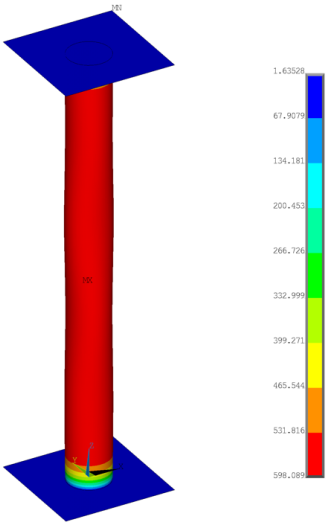

Figure 64 – Body temperature at the end of the simulation – HYDROCARBON **[26]** + 25%.

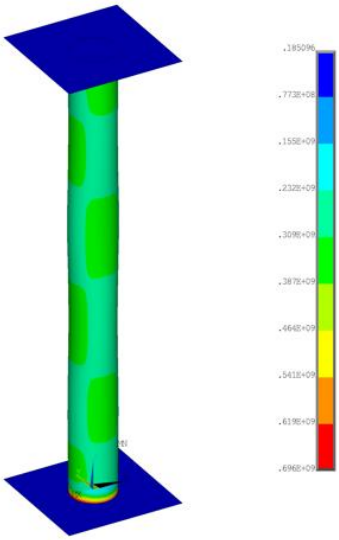

Figure 65 - Von Mises Stress at the end of the simulation (last time step) – HYDROCARBON **[26]** + 25%.

Figure 66 shows the displacement along the column length (z-axis) with the temperature varying according to the hydrocarbon curve **[26]** and a mechanical load of 477981 N applied in the driving plate. The fire resistance time was even lower compared to the previous one, as expected, around 1:48 minutes, with a failure temperature of 534 ºC, as depicted in **Figure 67**. **Figure 68** shows the Von Mises stress installed in the element at the last moment of the simulation.

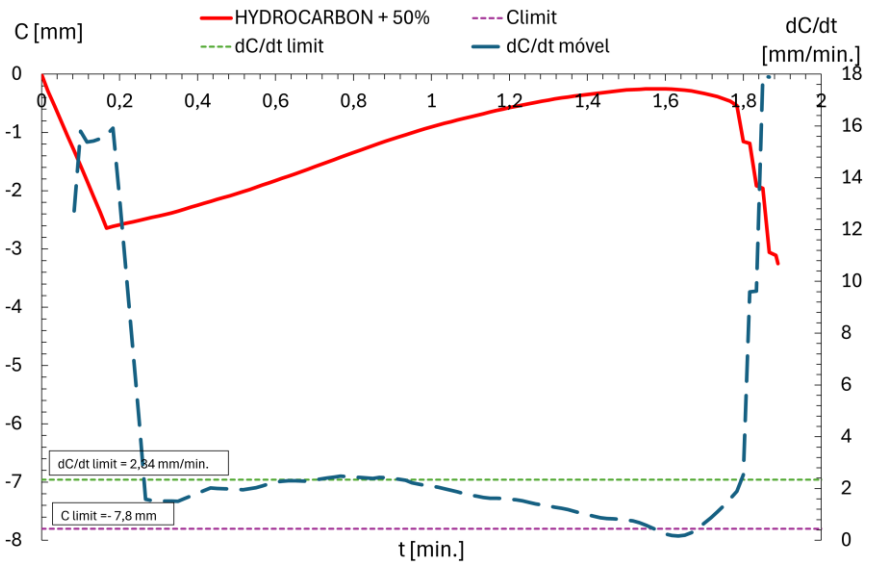

Figure 66 – Graph of displacement-time relationship for hydrocarbon fire curve + 50% of load bearing capacity at room temperature.

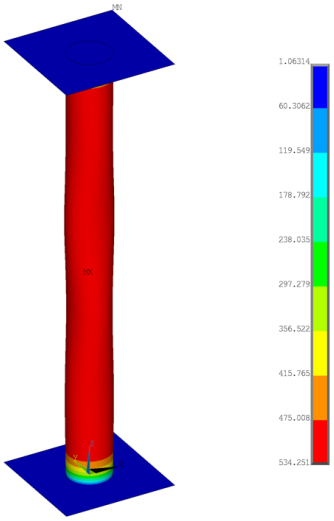

Figure 67 – Body temperature at the end of the simulation – HYDROCARBON **[26]** + 50%.

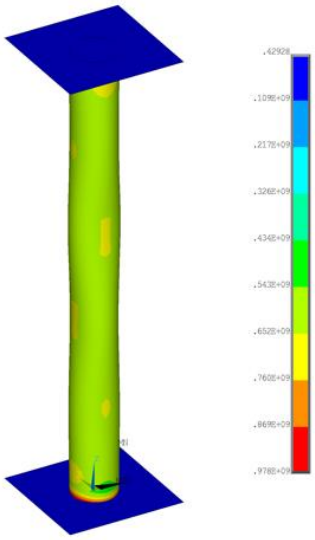

Figure 68 - Von Mises Stress at the end of the simulation (last time step) – HYDROCARBON **[26]** + 50%.

Figure 69 shows the displacement along the column length (z-axis) with the temperature varying according to the hydrocarbon curve **[26]** and a mechanical load of 716971.5 N applied in the driving plate. The fire resistance time was the lowest, as expected, around 1:24 minutes, with a failure temperature of 400 ºC, as can be shown in **Figure 70**. **Figure 71** shows the Von Mises stress installed in the element at the last moment of the simulation.

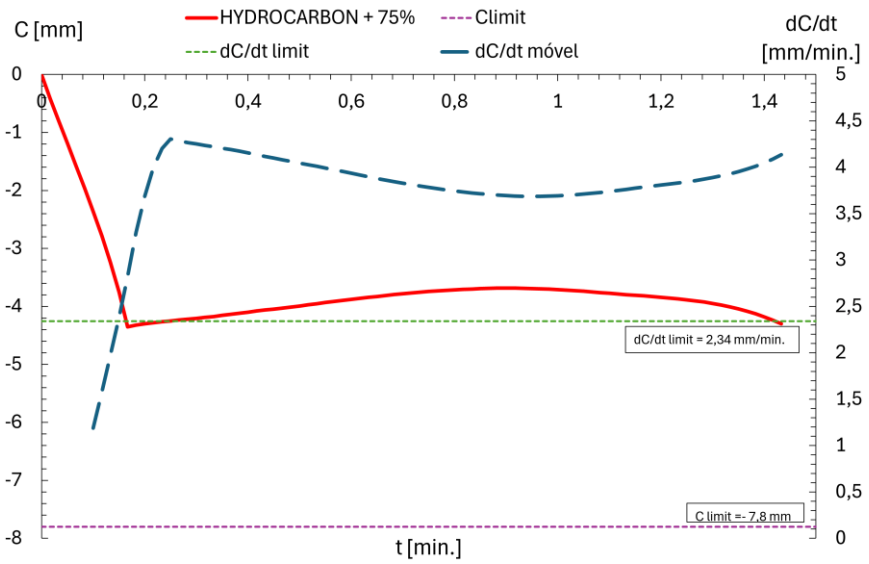

Figure 69 – Graph of displacement-time relationship for hydrocarbon fire curve + 75% of load bearing capacity at room temperature.

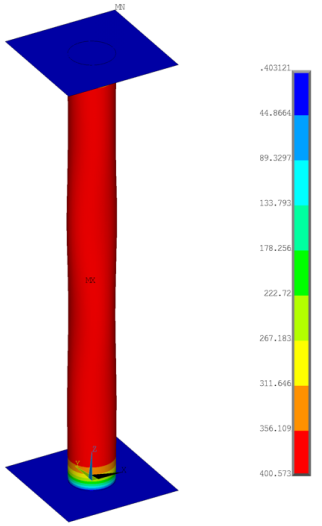

Figure 70 – Body temperature at the end of the simulation – HYDROCARBON **[26]** + 75%.

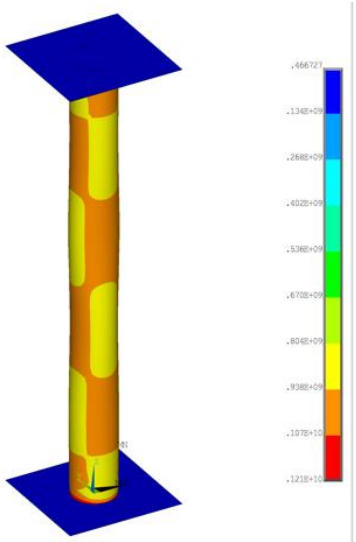

Figure 71 - Von Mises Stress at the end of the simulation (last time step) – HYDROCARBON **[26]** + 75%.

In all these cases, it was not possible to classify the column according to the EN 13501 standard **[28]**. The high temperature variation in steel occurring within the first few seconds, as dictated by the hydrocarbon fire curve, resulted in the column failing to withstand the required minimum of 15 minutes of fire resistance, lasting a maximum of only 2 minutes. Consequently, to render the column viable for use in a building requiring at least 15 minutes of fire resistance under these conditions, it is necessary to investigate an appropriate insulation method that would enable the column to withstand a hydrocarbon-induced fire scenario. The table summarizes the thermo-mechanical results.

Table 7 - Thermo-mechanical results (resume).

TEST	CRITICAL TEMPERATURE [ºC]	CRITICAL TIME [min.]	CLASSIFICATION – EN13501-2
ISO 834 + 25%	621	21	R20
ISO 834 + 50%	527	15	R15
ISO 834 + 75%	403	10	N/A
HYDROCARBON + 25%	598	2	N/A
HYDROCARBON + 50%	534	1:48	N/A
HYDROCARBON + 75%	400	1:24	N/A

5- CONCLUSIONS

By conducting all the proposed simulations, it was possible to increase the knowledge of existing information on the use of Ultra-High Strength Steels (UHSS) in buildings and their response to fire conditions. This study aimed to provide a deeper understanding of the behaviour of these materials under different fire scenarios (different heating rates).

The validation of the experimental study carried out by Farmani et al. **[3]** generated some results that did not fully agree with what was reported in the article. However, it could still provide information on the behaviour of the column under R5 and R20 heating rates, as reported in the study by Farmani et al. **[3]**.

The results demonstrated that mechanical load significantly affects the fire resistance duration of the element. Specifically, higher applied loads result in lower failure temperatures and reduced fire resistance.

For the analysis involving ISO 834 **[27]** and hydrocarbon fire curves **[24]**, the thermal properties provided by EN 1993-1-2 **[20]** were used and produced acceptable results. It is important to note that the effect of creep, which was not addressed in this study, should be included in the constitutive law for a more accurate analysis.

It can be concluded that the rate of temperature variation over time has a dominant parameter on the fire resistance time of the element compared to the applied mechanical load. This is evident from the simulation of the element subjected to the hydrocarbon curve, for example, where a rapid fire temperature increases within the first few seconds. As a result, the CHS column can withstand fire for only 2 minutes at best, even with just 25% of the applied load capacity, with the same load, and applying the ISO 834 **[27]** temperature curve, the element withstood 21 minutes, 10 times more than the previous mentioned. For its application in a building structure, it is recommended provide thermal insulation to the element. This would enhance its fire resistance, allowing it to withstand fire conditions for a longer duration and providing sufficient time for potential evacuation.

Finally, it is essential to conduct additional studies, including experimental tests and FE simulations to develop more information for various types of UHSS with more diverse geometries and sizes. This would enable a more precise comparison with the properties presented by the Standards and would help to understand even more about the behavior of this components in situations involving the safety of those who use it and depend on the good functioning of the structure when exposed to different conditions,

often, to emerge from these situations alive and intact.

BIBLIOGRAPHY

[1] L. Keränen, M. Kangaspuoskari e J. Niskanen, "Ultra-High-Strength steels at elevated temperatures", Journal of Constructional Steel Research, 2021.

[2] Mohammad Amin Farmani, Amin Heidarpour, Xiao-Ling Zhao. A distinctive approach to testing and modeling thermal creep in ultra-high strength steel, International Journal of Mechanical Sciences, Volume 198, 2021, 106362. https://doi.org/10.1016/j.ijmecsci.2021.106362.

[3] Mohammad Amin Farmani, Amin Heidarpour, Development of design equations for ultra-high strength steel CHS columns under transient fire conditions considering thermal creep and axial restraint effects, Fire Safety Journal, Volume 136, 2023, 103756, ISSN 0379-7112. https://doi.org/10.1016/j.firesaf.2023.103756.

[4] BS EN 1993-1-1. Eurocode 3: design of steel structures: Part 1–1: general rules and rules for buildings. London: BSI; 2005.

[5] BS EN 1993-1-12. Eurocode 3: design of steel structures: Part 1–12: additional rules for the extension of EN 1993 up to steel grades S700. London: BSI; 2007.

[6] AISC (American Institute of Steel Construction), Specification for Structural Steel Buildings, ANSI/AISC 360-16, Am. Inst. Steel Constr., 2016, p. 676.

[7] ABNT NBR 8800: 2008. *Projeto de Estruturas de Aço e de Estruturas Mistas de Aço e Concreto de Edifícios*, ABNT – Associação Brasileira de Normas Técnicas. Rio de Janeiro.

[8] GB 50017–2003 code for design of steel structures. Beijing: China Architecture & Building Press; 2006.

[9] Gang Shi, Huiyong Ban, Frans S.K. Bijlaard, Tests and numerical study of ultra-high strength steel columns with end restraints, Journal of Constructional Steel Research, Volume 70, 2012, Pages 236-247, ISSN 0143-974X. https://doi.org/10.1016/j.jcsr.2011.10.027.

[10] NOGUEIRA, Rosiane de Castro. Caracterização Mecânica E Análise Microestrutural Com A Utilização Da Técnica De Tríplice Ataque Do Aço Multifásico AISI 4350. 2013. 136 f. Tese (Doutorado) - Curso de Pós-Graduação em Engenharia Mecânica, Universidade Estadual Paulista, Guaratinguetá, 2013.

[11] LAJARIN, Sérgio Fernando. Influência Da Variação Do Módulo De Elasticidade Na Previsão Computacional Do Retorno Elástico Em Aços De Alta Resistência. 2012. 197 f. Tese (Doutorado) - Curso de Pós-Graduação em Engenharia Mecânica, Universidade Federal do Paraná, Curitiba, 2012.

[12] Andi Su, Yao Sun, Ou Zhao, Yating Liang. Local buckling of S960 ultra-high strength steel welded I-sections subjected to combined compression and major-axis bending. Engineering Structures, Volume 248, 2021, ISSN 0141-0296. https://doi.org/10.1016/j.engstruct.2021.113213.

[13] Fatemeh Azhari, Amin Heidarpour, Xiao-Ling Zhao, Christopher R. Hutchinson, Post-fire mechanical response of ultra-high strength (Grade 1200) steel under high temperatures: Linking thermal stability and microstructure, Thin-Walled Structures, Volume 119, 2017, Pages 114-125, ISSN 0263-8231. https://doi.org/10.1016/j.tws.2017.05.030.

[14] SSAB Manufacturing Company, ⟨https://www.ssab.com/⟩, in, Stockholm, Sweden, 1878. - Google Search, (n.d.). https://www.ssab.com/pt-br/marcas-e-produtos/hardox/programa-de-produto/400 (accessed October 17, 2023).

[15] F. Javidan, A. Heidarpour, X.L. Zhao, J. Minkkinen, Application of high strength and ultra-high strength steel tubes in long hybrid compressive members: experimental and numerical investigation, Thin Walled Struct. 102 (2016) 273–285, https://doi.org/10.1016/j.tws.2016.02.002.

[16] Fatemeh Azhari, Amin Heidarpour, Xiao-Ling Zhao, Christopher R. Hutchinson.

Mechanical properties of ultra-high strength (Grade 1200) steel tubes under cooling phase of a fire: An experimental investigation, Construction and Building Materials, Volume 93, 2015, Pages 841-850, ISSN 0950-0618. https://doi.org/10.1016/j.conbuildmat.2015.05.082.

[17] AS, AS 4100-1998 Rec:2016, Standards Australia, 1998th ed., 1998. Sydney, Australia.

[18] EN 1363-1:2020. "Fire Resistance tests, Part 1: General requirements". European Committee of Standardization, 2020.

[19] M. K. Thompson e J. M. Thompson, "ANSYS Mechanical APDL for Finite Element Analysis". Elsevier, 2017, ISBN: 978-0-12-812981-4.

[20] Ansys, ANSYS Mechanical APDL Element Reference, 2011.

[21] EN 10210-2 (2006). Hot finished structural hollow sections of non-alloy and fine grain steels – Part 2: Tolerances, dimensions and sectional properties.

[22] EN 10219-2 (2006). Cold formed welded structural hollow sections of non-alloy and fine grain steels – Part 2: Tolerances, dimensions and sectional properties.

[23] N. Vasios, "Nonlinear Analysis of Structures - The Arc Length Method: Formulation, Implementation and Applications", Harvard University, 2015.

[24] EN 1993-1-2 (2005). Design of steel structures – Part 1-2: General rules – Structural fire design.

[25] International Organization for Standardization, ISO 834-1: Fire-resistance tests – Elements of building construction – Part 1: general requirements, 1999.

[26] European Committee for Standardization, Eurocode 1 1991: Actions on structures - Part 1-2: General actions on structures exposed to fire, 2002.

[27] E. M. Fonseca, C. A. M. Oliveira e F. Q. Melo, "Validação Experimental de um

Modelo Teórico para Cálculo de Elevados Gradientes Térmicos em Estruturas de Parede Fina.", *APAET*, 2002.

[28] EN 13501-2 (2010). Fire classification of construction and building elements – Part 2: Classification using data from fire resistance testes, excluding ventilation services.